Marine Geology 457 (2023) 106994

Contents lists available at ScienceDirect

Marine Geology

journal homepage: www.elsevier.com/locate/margo

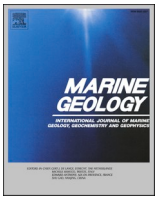

Staggered cold-water coral mound build-up on an Alboran ridge during the last deglacial (East Melilla Mound Field, western Mediterranean)

Robin Fentimen [a,1,*], Eline J. Feenstra [a], Andres Rüggeberg [a], Efraim Hall [a], Antonietta Rosso [b], Irka Hajdas [c], David Jaramillo-Vogel [a], Bernard Grobéty [a], Thierry Adatte [d], David Van Rooij [e], Norbert Frank [f], Anneleen Foubert [a]

[a] Department of Geosciences, University of Fribourg, Chemin du Musée 6, Fribourg, Switzerland
[b] Department of Biological, Geological and Environmental Sciences, University of Catania, Catania, Italy
[c] Laboratory of Ion Beam Physics, ETH Zurich, Otto-Stem-Weg 5, Zurich CH-8093, Switzerland
[d] Institute of Earth Surface Dynamics, University of Lausanne, Lausanne, Switzerland
[e] Department of Geology, Ghent University, Krijgslaan 281 S8, B9000, Gent, Belgium
[f] Institute of Environmental Physics, University of Heidelberg, Im Neuenheimer Feld 229, Heidelberg 69120, Germany

ARTICLE INFO

Editor: Michele Rebesco

Keywords:
Cold-water corals
Mediterranean Sea
Bølling-Allerød
Holocene
Benthic foraminifera
Palaeoclimate

ABSTRACT

The start-up, build-up and demise of cold-water coral mounds are governed by environmental changes at global, regional and local scales. Whilst the formation of cold-water coral mounds across the globe is widely documented to follow interglacial-glacial cycles, less is known about their response to local environmental fluctuations during short time intervals. This study investigates the local variations in coral mound build-up along Brittlestar Ridge I (East Melilla Coral Province, Southeast Alboran Sea) by comparing three on-mound gravity cores collected ~1 km apart, together with five previously described on-mound records, along a longitudinal transect on the ridge crest. Radiocarbon foraminiferal dating associated to U-series coral dating allowed to correlate the different records and to estimate mound aggradation rates, whilst grain-size analysis provided information on bottom current velocities. Prior to a rapid period of coral mound build-up initiated at ~14.75 ka BP, the three cores present an occurrence of cm-thick bryozoan-dominated intervals nearly entirely consisting of the erect cheleistome *Buskea dichotoma*. Offsets between benthic foraminiferal and coral ages suggest that older dead allochtonous benthic foraminifera are possibly eroded from neighbouring settings, transported and deposited within the coral framework. In contrast, younger benthic foraminifera would develop on dead coral framework during periods of reef stagnation. The comparison of all cores indicates that mound build-up along the ridge did not follow the same timing during the last ~16 kyr and that mound aggradation was marked by a staggered dynamic. Both local differences in bottom current velocities and patchiness of other key environmental actors (e.g. substrate availability) are suspected to drive the observed staggered mound build-up. Cold-water coral mound build-up shows important differences during Greenland Interstadial 1 (i.e. the Bølling-Allerød) and the Holocene, hence examplifying how local environmental variability may overprint global and regional climate variability over short time periods.

1. Introduction

Living scleractinian cold-water coral (CWC) ecosystems are found worldwide and are known to form mound structures along continental margins (e.g. Roberts et al., 2006). CWCs are most abundant at depths shallower than 1500 m and within water masses that display salinity values around 35 PSU and temperatures between 4 and 14 °C (Freiwald, 2002; Freiwald et al., 2004; Roberts et al., 2006; Davies and Guinotte, 2011; Flögel et al., 2014). Cold-water corals thrive in areas of enhanced primary productivity (White et al., 2005; Wienberg et al., 2010; Eisele et al., 2011; Fink et al., 2013, 2015; Stalder et al., 2015, 2018), whilst their development is driven by locally increased current velocity and turbulence, which increase food availability to the corals (i.e. higher particle encounter rates, resuspension of organic matter) (Rüggeberg

* Corresponding author.
E-mail address: robin.fentimen@univ-angers.fr (R. Fentimen).
[1] Present address: CNRS, UMR 6112, Laboratoire de Planétologie et Géosciences, Université d'Angers, 49000, Angers, France.

https://doi.org/10.1016/j.margeo.2023.106994
Received 22 May 2022; Received in revised form 5 January 2023; Accepted 11 January 2023
Available online 13 February 2023

et al., 2005; White et al., 2005; Dorschel et al., 2007; Mienis et al., 2007; Davies et al., 2008). Under suitable environmental conditions, CWCs can form mounds comprised of CWC skeletons, embedded in a matrix of hemipelagic sediments that stabilize the structure (Foubert et al., 2008; Titschack et al., 2009; Thierens et al., 2010). The height of these build-ups ranges from several to hundreds of metres, whereas their base can extend for several kilometres (De Mol et al., 2002; Huvenne et al., 2003; Dorschel et al., 2005; Wheeler et al., 2007). Large CWC mound provinces have for example been observed in the Northeast Atlantic off the coast of Ireland (De Mol et al., 2002; Huvenne et al., 2002; Wheeler et al., 2007; Van der Land et al., 2013), Norway (Freiwald, 2002; López Correa et al., 2012; Sneli, 2014), Morocco (Foubert et al., 2008; Wienberg et al., 2010; Hebbeln, 2019), Mauritania (Ramos et al., 2017; Wienberg et al., 2018), Mexico (Hebbeln et al., 2014; Matos et al., 2017), and in Mediterranean basins (Remia and Taviani, 2005; Freiwald et al., 2009; Comas and Pinheiro, 2007; Martorelli et al., 2011; Fink et al., 2013; Lo Iacono et al., 2014; Corbera et al., 2019; Angeletti et al., 2020; Camafort et al., 2020; Corbera et al., 2022). In the Northeast Atlantic Ocean and the Mediterranean Sea, the main framework building azooxanthellate scleractinian corals are *Desmophyllum pertusum,* formely known as *Lophelia pertusa* (Addamo et al., 2016), and *Madrepora oculata* (e.g. Freiwald, 2002; Roberts et al., 2006, 2009).

Frank et al. (2011) proposed that the biogeographic limit of framework-forming CWCs is controlled by glacial-interglacial cycles. Along the Irish margin, CWCs flourish during interglacial periods (Dorschel et al., 2005; Rüggeberg et al., 2007; Frank et al., 2011), whilst in the Gulf of Cádiz they rather thrive during glacial periods (Wienberg et al., 2009, 2010). In the southern Northeast Atlantic, along the Mauritanian margin, CWC mound build-up occurred essentially during the last glacial period, though shallower mounds in the area also experienced periods of build-up during the last interglacial period (Eisele et al., 2011; Wienberg et al., 2018). Documented CWC occurrences in the Mediterranean demonstrate that they mostly thrive during warm intervals (Fink et al., 2015 and references therein; Wang et al., 2019; Krengel, 2020; Corbera et al., 2021), although recent observations show that corals situated within the Tunisian Coral Mound Province experienced their most important growth phase during the last glacial period (Corbera et al., 2022). In the Mediterranean Sea, CWC mounds are found in the Alboran Sea (Comas and Pinheiro, 2007; Fink et al., 2013; Lo Iacono et al., 2014; Corbera et al., 2019; Hebbeln, 2019; Sánchez-Guillamón et al., 2022), on the Tunisian Plateau (Camafort et al., 2020; Corbera et al., 2022), the Strait of Sicily (Martorelli et al., 2011), in the northern Ionian Sea (Carlier et al., 2009; Freiwald et al., 2009) and in the Corsica Channel (Remia and Taviani, 2005; Angeletti et al., 2020). CWC mounds situated in the Alboran Sea are currently divided between those in the West and East Melilla Coral Provinces (WMCP and EMCP) off the coast of Melilla (Comas and Pinheiro, 2007; Fink et al., 2013; Lo Iacono et al., 2014), and those located on the Cabliers Bank (the Cabliers Coral Mound Province: CMP), which is ~40 km northeast of the EMCP (Schröder-Ritzrau et al., 2005; Pardo et al., 2011; Corbera et al., 2019; Fig. 1). Only the North CMP hosts living coral communities at their surface, whereas the other Alboran CWC mounds are currently in a stagnation phase (Corbera et al., 2019; Hebbeln, 2019; Sánchez-Guillamón et al., 2022).

A number of studies report that recent phases of mound build-up at the EMCP took place between 14.6 and 13.5 ka BP and during the Early to Mid-Holocene, whilst it stagnated during the Younger Dryas (Fink et al., 2015; Stalder et al., 2015; Wienberg, 2019; Krengel, 2020). Coral proliferation is thought to be predominantly related to increased fluxes of organic matter (Fink et al., 2013; Stalder et al., 2015, 2018; Fentimen et al., 2020a). Fink et al. (2013) and Corbera et al. (2021) linked the temporal distribution of CWC development, respectively at Brittlestar Ridge I (BRI) and at the CMP, to enhanced primary productivity associated with the deposition of Organic Rich Layer 1 in the western Mediterranean (Cacho et al., 2002; Pérez-Folgado et al., 2004; Jimenez-Espejo et al., 2007; 2008; Rogerson et al., 2008; Rodrigo-Gámiz et al., 2011). Organic Rich Layer 1 is linked to higher surface water productivity (Bárcena et al., 2001; Ausín et al., 2015) and changes in deep-water ventilation (Cacho et al., 2002; Jimenez-Espejo et al., 2008; Rogerson et al., 2008). Stalder et al. (2015, 2018) and Fentimen et al. (2020a) proposed that increased surface productivity associated with both enhanced Atlantic Water inflow and continental runoff promoted

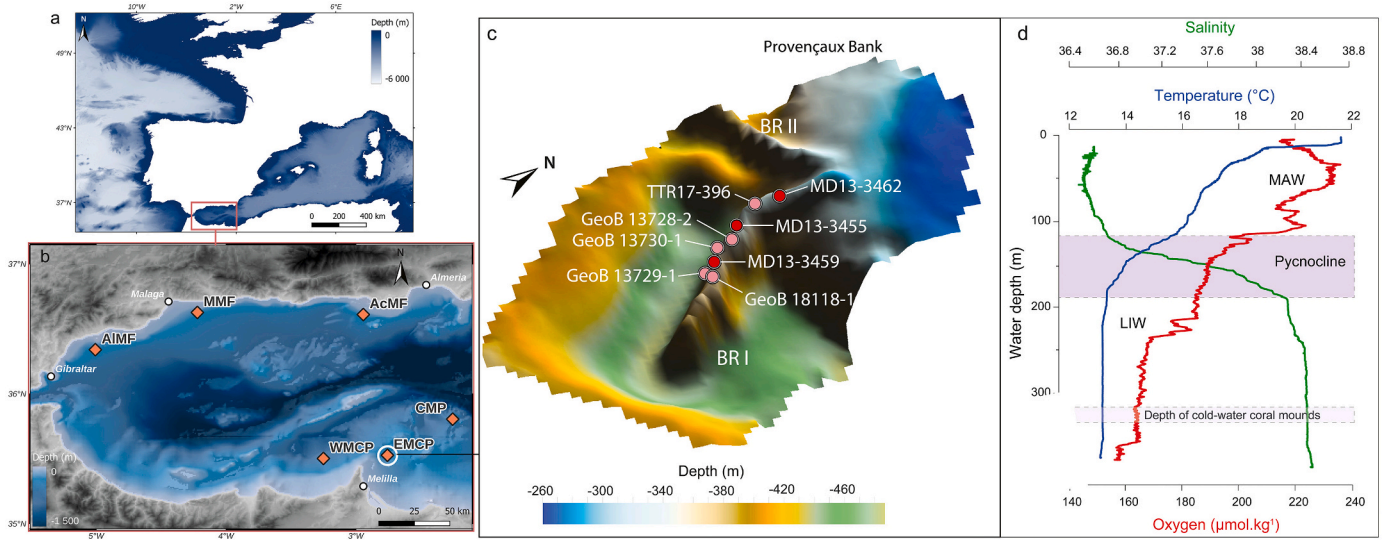

Fig. 1. (a) Location of the Alboran Sea (orange rectangle); (b) location of the East Melilla Coral Province (EMCP), West Melilla Coral Province (WMCP), Cabliers Coral Mound Province (CMP), Aceitunas carbonate Mound Field (AcMF), Málaga carbonate Mound Field (MMF), and Alcántara carbonate Mound Field (AlMF); (c) 3D view of the Brittlestar Ridge I area within the East Melilla Coral Province and position of the three gravity cores MD13-3455G, MD13-3459G and MD13-3462G retrieved during EUROFLEETS cruise MD194 Gateway on board RV *Marion Dufresne II* (red dots). Other coral-bearing gravity cores from Brittlestar Ridge I used in this study, namely GeoB 13,728–2, GeoB 13,729–1 and GeoB 13,730–1 (Fink et al., 2013), GeoB 18,118–1 (Wienberg et al., 2022), and TTR17-396G (Stalder et al., 2018) are also indicated (pink dots). Contour depth expressed in meters (10 m interval lines); (d) profile of water temperature, salinity and oxygen content above Brittlestar Ridge I taken on the 14th of June 2013 (Van Rooij et al., 2013). The location of the pycnocline (separation between Modified Atlantic Water (MAW) and Levantine Intermediate Water (LIW) is indicated by the purple box. (For interpretation of the references to colour in this figure legend, the reader is referred to the web version of this article.)

coral growth at the EMCP. The aforementioned studies also suggest that water mass configuration may play a major role. Wang et al. (2019) proposed that water mass configuration, specifically internal waves occurring at the interface between two water masses and propagating along the pycnocline (Pomar et al., 2012), are an important driver for CWC growth at the WMCP (Wang et al., 2019). Indeed, internal waves are a potential source of turbulent energy and accumulate particulate organic matter (Puig et al., 2004; McCave, 2009; Pomar et al., 2012), both essential for the development of coral communities.

Although the development of CWCs during the last 15 kyr at the EMCP is well constrained, little is yet known about the temporal variability and timing of CWC mound formation at a local scale (ca. 3 km). The objective of this study is to highlight these local disparities in CWC mound development through the combined investigation of three on-mound gravity cores located approximately 1 km apart from each other on Brittlestar Ridge I (BRI, EMCP), and their comparison to five other on-mound cores described from the area.

2. Regional setting

2.1. Geology and oceanography of the Alboran Sea

The Alboran Sea is the westernmost part of the Mediterranean Sea (Fig. 1a), bounded by the Iberian Peninsula to the north and Morocco to the south. This Sea is a 350 km long (W-E) and 150 km wide (N-S) extensional basin with a maximum depth of 1800 m (Comas et al., 1999; Ercilla et al., 2016), which connects to the west with the Atlantic Ocean by the Strait of Gibraltar and to east with the Algerian Basin. Its seafloor morphology is complex, comprising sub-basins, ridges, plateaus, troughs and seamounts (Comas et al., 1999), with one of the most prominent tectonic features being the NE to SW Alboran Ridge (Martínez-García et al., 2013). This geomorphic feature divides the Alboran Sea into the Motril (northern), eastern, southern and western sub-basins (Ercilla et al., 2016; Juan et al., 2016). Besides its complex geomorphology, the Alboran Sea is also characterized by the presence of large Pliocene and Quaternary contourites (Hernández-Molina et al., 2011; Ercilla et al., 2016; Juan et al., 2016).

The Mediterranean Sea is governed by a deep-overturning circulation, consisting of a flux of relatively fresh Modified Atlantic Water (MAW) and salty Mediterranean Outflow Water (MOW), flowing below the former, respectively entering and exiting the Mediterranean (Schroeder et al., 2012; Tanhua et al., 2013). After entering the western Mediterranean, MAW establishes a quasi-permanent anti-cyclonic gyre in the west and a more variable circuit in the east of the Alboran Sea (Millot, 1999). It forms a 100–200 m layer, flowing on the surface and characterized by a salinity increase from Gibraltar to the east due to evaporation and mixing. MAW and Levantine Intermediate Water (between ~200 and 1000 m; LIW) are the two main water masses of the shallow circulation cell of the Mediterranean (Millot, 1999). LIW is formed in the eastern Mediterranean and transits towards the western Mediterranean, before exiting as MOW through the Strait of Gibraltar. Exiting MOW has direct implications on the stability of North Atlantic Meridional Overturning Circulation (Tanhua et al., 2013). Below the LIW, the Eastern and Western Mediterranean Deep Waters are the deepest flowing water masses in the Mediterranean (Millot, 1999).

2.2. The East Melilla Coral Province

The Melilla Mound Field, situated in the Southeast Alboran Sea, is separated between the EMCP and WMCP (Fig. 1b). Brittlestar Ridge I is located in the northern part of the EMCP and is one of the three ridges (I, II and III) connected to the shallow (~200 m deep) Provençaux Bank volcanic plateau (Fig. 1c; Ammar et al., 2007; Comas and Pinheiro, 2007). The ridges are accompanied by distinct erosional moats surrounding their base (Hebbeln, 2019; Fig. 1c), likely created by strong bottom currents (Comas and Pinheiro, 2007). Brittlestar Ridge I is ~3 km long and rises between 50 and 150 m above the surrounding seafloor (Hebbeln, 2019; Fig. 1c). At present, CWC mounds on BRI occur well within the envelope of LIW in water temperatures of about ~13.2 °C, absolute salinity of ~38.4 g/kg and dissolved oxygen of ~163 μmol kg^{-1} (Fig. 1d), whilst MAW flows above LIW with the pycnocline situated between ~100 and 200 m water depth (Fig. 1d). Remotely operated vehicle video observations along the ridge reveal only small and scarce living CWC colonies and predominantly dead CWCs (Hebbeln, 2019).

3. Materials and methods

3.1. Sample collection

During EUROFLEETS cruise MD194 "Gateway" on board the RV *Marion Dufresne II,* three gravity cores, MD13-3462G, MD13-3455G and MD13-3459G, were retrieved from the crest of BRI (Table 1; Fig. 1c). For the purpose of this study, we have investigated the full extent of cores MD13-3455G and MD13-3459G and solely the first 70 cm of core MD13-3462G since these sections cover the same time period, as evidenced by the radiometric coral, foraminiferal and bryozoan ages (see sections 3.5 and 4.1). Potential temperature (°C), salinity and oxygen content (μmol kg^{-1}) of water masses in the EMCP region were obtained using the on-board conductivity-temperature-depth (CTD) profiler of the RV *Marion Dufresne II* (Fig. 1d) at the following coordinates: 35°26.087′N, 2°30.100′W.

3.2. Computed tomography and image analyses

The volume percentage of CWCs, bryozoans, bivalves and brachiopods were calculated by X-ray Computed Tomography (CT) for all three cores. X-ray CT imaging was performed on whole-round core sections with the *Somatom Definition AS64* (Siemens®, Forchheim, Germany) at the Institute of Forensic Sciences at the University of Bern (Switzerland). Measurements used a tube voltage of 120 kV and images were reconstructed with a horizontal resolution of 0.3 mm and a slice thickness of 0.6 mm taking into account an increment of 0.3 mm, which results in a vertical spatial resolution of 0.3 mm. The horizontal resolution of the reconstructed images is 0.3 mm. Prior to segmentation, images were filtered using a non-local means filter. Hierarchical watershed segmentation of the coral and bryozoan fragments, followed by labelling and quantitative analyses, were performed with the Avizo 9.4 software. Fragments other than CWC and bryozoan skeletal clasts were segmented manually. Estimations of the volume percentage were performed on each integrated slice. The two dominant scleractinian coral species *D. pertusum* and *M. oculata* were not distinguished; hence relative abundances of these two species were estimated during the core descriptions (see below).

3.3. Core descriptions

Cores were split frozen and sedimentary facies descriptions were done at the University of Fribourg (Switzerland) prior to sampling. Sediment colour was defined following a Munsell Soil Colour chart. Major macrofaunal elements were also identified (corals, bryozoans, bivalves and brachiopods) down to species level when possible (noticeably for corals). The relative proportions of *D. pertusum* and *M. oculata* within the cores were estimated visually and are thus semi-quantitative. The preservation state of CWC skeletons was defined following their degree of dissolution, breakage and bioerosion. A good preservation state corresponds to corals which demonstrate solid theca walls with a good preservation of their internal structures, and neither signs of breakage nor of dissolution or bioerosion (e.g. boring, grooves, fungal and sponge traces). Corals with a medium preservation show signs of bioerosion, yet their theca walls are still robust. In contrast, poorly preserved corals demonstrate important signs of bioerosion resulting in weaker theca walls and may show signs of breakage.

Table 1
Coordinates, core recovery (cm), depth (m) and studied interval for this study (cm) of gravity cores retrieved on Brittlestar Ridge I (BRI; Alboran Sea) during the EUROFLEETS cruise MD194 Gateway on board RV *Marion Dufresne II* (Van Rooij et al., 2013).

Core	Latitude	Longitude	Recovery (cm)	Depth (m)	Studied interval (cm)
MD13-3455G	35°26.337′N	2°30.926′W	491	319	491
MD13-3459G	35°26.182′N	2°30.807′W	752	330	752
MD13-3462G	35°26.531′N	2°31.073′W	926	327	70

3.4. Grain size analysis

Samples were taken using a small spatula every 5 cm for all three cores. Grain size was determined on the siliciclastic fraction for all three cores using the Malvern Mastersizer 3000 at the Department of Geology at Ghent University. Large coral, bryozoan and shell fragments were first hand picked out of each sample. To remove organic matter, samples were boiled in 35% H_2O_2 until the reaction stopped and then placed for ~2 min in 10% HCl to dissolve carbonates. Prior to measurements, all samples were boiled in 2% sodium polymetaphosphate to insure total particle separation. A 2 mm mesh sieve placed above the receiver of the Malvern Mastersizer 3000 retained any remaining large particles. Samples were measured three times and an average value was taken as the final result. The sortable silt mean grain size ($\bar{SS}$; i.e., the mean of the 10–63 μm size fraction; McCave et al., 1995) was calculated for all cores and a paired Student *t*-test was carried out to compare $\bar{SS}$ distributions of cores MD13-3455G and MD13-3459G. End-member modelling of grain-size data was performed using the EMMAgeo package for R (Dietze and Dietze, 2019). The number of end-members was identified thanks to the *test.robustness()* function provided by the EMMAgeo package.

3.5. Uranium-series and radiocarbon dating

Nine U-series isotope measurements were carried out on two different framework-forming scleractinian coral species (*D. pertusum* and *M. oculata;* Table 2). Prior to measurements, the CWC skeletal fragments were mechanically cleaned using a sand blasting method and chemically cleaned using weak acid leaching as described by Frank et al. (2004), Douville et al. (2010), Matos et al. (2015) and updated by Wefing et al. (2017). The measurements were conducted at the Institute for Environmental Physics at Heidelberg University (Germany) in 2017. The U-series isotope measurements were done by multi-collector inductively coupled plasma mass spectrometry (*ThermoFisher Neptune Plus*; Wefing et al., 2017). Blanks were smaller than 0.4 fg for ^{234}U and 0.04 fg for ^{230}Th. Ages were calculated using the half-lives of Cheng et al. (2000), corrected for initial Th using a $^{230}Th/^{232}Th$ ratio of 8.0 ± 4.0 and presented in kiloyears before present (ka BP; P = 1950 CE). Lastly, age uncertainties were quoted at the 2σ confidence level, not including half-life uncertainties. Integrated to this study are also 6 U-series isotope measurements previously published by Fentimen et al. (2020a).

Radiocarbon dating was performed at the ETH in Zürich (Switzerland) on large (>250 μm) pristine/well-preserved (i.e. no breakage, no traces of dissolution and no boring) epibenthic foraminifera (*Cibicides refulgens*, *Discanomalina coronata* and *Lobatula lobatula*) and on one bryozoan (*Buskea dichotoma*) fragment from core MD13-3462G (Table 3). A total of thirteen foraminiferal samples were analysed from the three cores (Table 3). For each sample, foraminifera were picked to obtain 4 to 10 mg of pure carbonate. Prior to measurements, epibenthic foraminifera and the *B. dichotoma* fragment were cleaned in an ultrasonic bath and then dissolved in phosphoric acid. The extracted carbon dioxide was converted to graphite. A more detailed description of the preparation technique is given in Hajdas (2008). The ^{13}C-corrected radiocarbon ages were calibrated using the software *CALIB REV7.1.0* (Stuiver and Reimer, 1993; Stuiver et al., 2019), the MARINE13 calibration curve (Reimer et al., 2013) and a reservoir age correction of 390 ± 80 years (Siani et al., 2000; McCulloch et al., 2010). Calibrated ages are presented in calendar years before present (cal. Yrs. BP; P = 1950 CE) with a upper and lower 2σ confidence level and have been rounded to the next decennial. In addition to the samples dated here, 5 benthic foraminiferal radiocarbon ages previously published by Fentimen et al. (2020a) have also been integrated in this study.

Vertical mound aggradation rates (cm kyr^{-1}) were calculated based on benthic foraminiferal radiocarbon ages (ka BP) and on the U-series CWC ages (ka BP) following the approach used by Frank et al. (2009). Whilst the aggradation rates calculated from U-series CWC ages truly represent the rate of coral build-up, the rates calculated from the benthic foraminiferal radiocarbon ages rather reflect the rate of sediment accumulation within the framework. In the following text, both aggradation rates will be discussed and noted MAR_C (calculated from U-series CWC ages) and MAR_F (calculated from radiocarbon benthic foraminiferal ages).

4. Results

4.1. Chronostratigraphy

The stratigraphic framework and correlation of the core sections are based on the U-series coral and radiocarbon foraminiferal and bryozoan ages and follow the INTIMATE event stratigraphy (Rasmussen et al., 2014; see Tables 2 and 3). A major boundary can be distinguished at the base of all three core sections and is marked by the passage from a bryozoan-dominated to a coral-dominated interval (Figs. 2 and 3). Coral and foraminiferal ages indicate that this boundary corresponds to the onset of Greenland Interstadial 1 (GI-1, 14.69 to 13.10 ka; Tables 2 and 3; Fig. 3), hence implying that the bryozoan-dominated intervals at the base of cores MD13-3455G and MD13-3459G date back to Greenland Stadial 2.1 (GS-2.1, 22.90 to 14.69 ka; Fig. 3). In contrast, the bryozoan-dominated interval in core MD13-3462G is older and dates back to Greenland Stadial 3 (GS-3, 27.54 to 23.34 ka; Fig. 3), as demonstrated by the foraminiferal and bryozoan ages at 37 cm depth (26.220 and 26.315 ka BP respectively; Table 3; Fig. 3). Thus, the later core presents a hiatus of approximately 12 kyr at the contact between GS-3 and GI-1. The observed absence of erosive and/or gravitational-induced sedimentary features in split-cores and CT-scans at this boundary (Fig. 2) indicates that this interval was marked by a halt in mound-build, rather than a removal of mound sediments by erosive or mass wasting events.

One coral age places the onset of the Holocene at 87 cm depth in core MD13-3459G (Fig. 3, Table 2). Due to the scarceness of material, such a precise dating of Holocene deposits was unfeasible in both cores MD13-3455G and MD13-3462G (Fig. 3). However, based on foraminiferal and coral ages, it was possible to limit the onset of the Holocene to an interval between 13 and 35 cm, and 3 and 36 cm, in respectively MD13-3455G and MD13-3462G (Fig. 3, Table 2). The GI-1/Holocene boundary was then refined by correlating the three cores through comparison of their grain size records ($\bar{SS}$, $\bar{GS}$ and end-members; Fig. 3; section 4.3). Coral and foraminiferal ages demonstrate that Greenland Stadial 1 (GS-1, 12.90 to 11.70 ka; i.e. Younger Dryas) deposits are absent or extremely reduced in cores MD13-3455G and MD13-3462G (Fig. 3) and that a sedimentary hiatus between GI-1 and Holocene deposits exists in both cores. The absence or not of GS-1 deposits in core MD13-3459G cannot be determined based on coral and foraminiferal ages (Fig. 3), though the lack of any change in matrix sediment colour, texture and macrofaunal content between 172 and 87 cm would suggest that GS-1

Table 2
Details of Uranium-series isotope measurements carried out on 13 coral fragments. All errors are 2σ of the mean analytical uncertainty. Ratios determined using a Th—U spike calibrated to a secular equilibrium reference material (HU-1 at the IUP). Uncorrected, closed-system age calculated using the decay constants of Jaffey et al. (1971) for ^{238}U and of Cheng et al. (2000) for ^{230}Th and ^{234}U. Ages are reported relative to the date of analysis, from year 2018 and do not include uncertainties associated with decay constants. *Raw age. **Ages are corrected for the influence of seawater and/or detrital derived ^{230}Th using a ^{230}Th/^{232}Th ratio of 8 ± 4. Ages refer to the year 1950. Dp = *Desmophyllum pertusum*, Mo = *Madrepora oculata*. *Ages used to calculate mound aggregation rates (MAR_C). (1)Previously published in Fentimen et al. (2020a).

LAB ID	Core	Depth (cm)	S	Age* (ka)	±	Age** (ka)	±	^{238}U (μg/g)	±	^{232}Th (ng/g)	±	$\delta^{234}U$ (‰)	±	$\delta^{234}U_i$ (‰)	±
IUP- 8487*(1)	MD13-3455G	1	Mo	2.410	0.009	2.328	0.013	3.655397	0.000090	0.21536	0.00054	147.75	0.43	148.75	0.43
IUP- 8488*(1)	MD13-3455G	13	Dp	6.853	0.018	6.759	0.024	3.21046	0.00011	0.34916	0.00071	146.88	0.58	149.74	0.59
IUP- 8489*(1)	MD13-3455G	35	Dp	13.810	0.049	13.725	0.049	3.40376	0.00010	0.24464	0.00073	144.02	0.56	149.75	0.59
IUP- 8490*(1)	MD13-3455G	280	Dp	14.582	0.049	14.501	0.054	3.21414	0.00010	0.18802	0.00050	143.12	0.54	149.13	0.56
IUP- 8491(1)	MD13-3455G	328	Dp	14.603	0.051	14.519	0.052	3.29380	0.00009	0.22973	0.00072	144.44	0.58	150.52	0.60
IUP- 8492*(1)	MD13-3455G	446	Dp	14.829	0.051	14.747	0.052	3.27789	0.00013	0.20500	0.00061	145.34	0.75	151.55	0.78
IUP- 8493*	MD13-3459G	5	Mo	3.775	0.020	3.693	0.021	3.49828	0.00010	0.20220	0.00071	147.39	0.59	148.96	0.60
IUP- 8494*	MD13-3459G	18	Dp	9.749	0.034	9.662	0.043	3.60786	0.00012	0.2998	0.00100	145.56	0.59	149.62	0.60
IUP- 8495	MD13-3459G	36	Dp	9.865	0.033	9.777	0.036	3.063028	0.000074	0.26129	0.00072	146.88	0.65	151.03	0.67
IUP- 8496*	MD13-3459G	87	Mo	11.380	0.039	11.267	0.042	3.91055	0.00012	0.7267	0.00210	145.17	0.59	149.90	0.61
IUP- 8497*	MD13-3459G	248	Dp	13.221	0.043	13.138	0.043	2.498983	0.000079	0.15586	0.00036	145.71	0.63	151.25	0.65
IUP- 8498*	MD13-3459G	447	Dp	13.732	0.037	13.646	0.039	3.24112	0.00011	0.24557	0.00048	143.21	0.45	148.87	0.47
IUP- 8499*	MD13-3459G	729	Dp	14.725	0.075	14.650	0.075	3.15610	0.00016	0.09499	0.00047	146.27	0.83	152.49	0.86
IUP- 8500	MD13-3462G	3	Mo	6.345	0.029	6.253	0.030	4.33769	0.00037	0.4311	0.00140	147.22	0.66	149.88	0.67
IUP- 8501	MD13-3462G	36	Dp	14.329	0.047	14.238	0.049	3.43669	0.00012	0.32542	0.00084	145.33	0.64	151.33	0.67

deposits are also absent or greatly reduced (Fig. 2). It may additionally be noted that the absence of GS-1 deposits is a commonly observed feature in the EMCP, WMCP and southern CMP (Fig. 4; Fink et al., 2013; Wang et al., 2019; Corbera et al., 2021).

Coral ages demonstrate that core MD13-3459G covers the entire GI-1 period from 14.69 to 12.90 ka, whilst core MD13-3455G covers only the Early GI-1 from 14.69 to 13.66 ka (Fig. 3). Similar to the 12 kyr hiatus in core MD13-3462G, there is no evidence of erosive or mass wasting sedimentary features at the transition from Early GI-1 to the Holocene in core MD13-3455G. Based on these observations, this late GI-1 hiatus in core MD13-3455G would correspond to a stagnation in mound build-up. In contrast to cores MD13-3455G and MD13-3459G, MD13-3462G covers little of GI-1 (Fig. 3). In the following text, GI-1 will be divided between "Early GI-1" (from 14.69 to 13.66 ka) and "Late GI-1" (from 13.66 to 12.90 ka). Taken together, the cores MD13-3455G (for Early GI-1 only) and MD13-3459G offer a high-resolution record of GI-1 (Fig. 3).

4.2. Macrofaunal content and mound aggradation rates

The sediment in cores MD13-3462G, MD13-3455G and MD13-3459G is composed of intervals containing varying amounts of mostly well-preserved aragonitic CWCs together with other bioclasts, such as bryozoans, gastropods, bivalves and brachiopods, in a mixed, clay- to sand-sized carbonate/siliciclastic matrix (Figs. 2 and 3). Well-preserved remains of the erect cheilostome bryozoan species *B. dichotoma* dominate the fauna during GS-3 and GS-2.1 (Figs. 2 and 3), with the highest bryozoan abundance being reached during GS-3 in core MD13-3462G (Fig. 3). During these time periods, bryozoan abundance varies between approximately 5 and 65 vol% (Fig. 3). In contrast, bryozoans are much more scarcely represented during GI-1 and the Holocene (between 0 and 20 vol%; Fig. 3). *Buskea dichotoma* accounts for >93% of the bryozoan associations in each sample, whereas *Palmiskenea gautieri*, *Reteporella sparteli* and a few other rigid erect species are scarcely represented. The *B. dichotoma*-dominated interval is thicker in cores MD13-3455G and MD13-3462G (respectively 40 and 30 cm thick) than in core MD13-3459G (15 cm thick; Figs. 2 and 3).

Directly above the *B. dichotoma*-dominated intervals, *D. pertusum* coral "units" (ca. 20 to 40 vol%) alternate with clayey intervals (Fig. 3) until the Mid to Late Holocene, at which point all three cores are characterized by a change in coral dominance from *D. pertusum* to *M. oculata* (at ca. 3, 18 and 20 cm in respectively cores MD13-3462G, MD13-3455G and MD13-3459G; Tables 2 and 3; Fig. 3). *Madrepora oculata* is absent within the *D. pertusum* "units", whereas it becomes dominant above with rare accessory occurences of *D. pertusum* (Figs. 2 & 3). Corals are better preserved in core MD13-3455G than in the two other cores, which show medium or even some parts of poor preservation in core MD13-3462G (Fig. 2). *Madrepora oculata* fragments are generally smaller and moderately well preserved. Core descriptions and CT-data show that CWCs are mostly preserved in living position, with little coral rubble. Corals and bryozoans are occasionally colonized by encrusting bryozoans, serpulids and to a lesser extent epibenthic foraminifera and molluscs.

Mound aggradation rates calculated from coral ages (MAR_C) vary between 2 and 675 cm kyr^{-1}, while those calculated from benthic foraminiferal ages (MAR_F) fluctuate between 22 and 480 cm kyr^{-1} (Fig. 4). Highest values of MAR_C (675 cm kyr^{-1}) and MAR_F (480 cm kyr^{-1}) are both recorded during Early GI-1 in core MD13-3455G and MD13-3459G respectively (Fig. 4). The lowest MAR_F (2.6 cm kyr^{-1}) is observed during the Holocene in core MD13-3459G (Fig. 4). MAR_F and MAR_C share the same descending trend from GI-1 to the Holocene, with mound aggradation stagnating during the Holocene in all three cores (Fig. 4). Low MAR_F are also recorded for GS-2.1 (Fig. 4).

Table 3
Radiocarbon ages of epibenthic foraminifera (*Lobatula lobatula, Cibicides refulgens* and *Discanomalina coronata*) and of a bryozoan fragment (*Buskea dischotoma*). Ages are corrected for a reservoir age of 390 ± 80 years (Siani et al., 2000). *Ages used to calculate mound aggregation rates (MAR_F). (1) Previously published in Fentimen et al. (2020a).

LAB ID	Core	Depth (cm)	Material	^{14}C age (years BP)	±1σ	2σ lower (years BP)	2σ upper (years BP)	2σ median (years BP)
ETH-87756*(1)	MD13-3455G	37	foraminifera	12,273	30	13,170	13,510	13,350
ETH-87755*(1)	MD13-3455G	157	foraminifera	13,033	35	13,900	14,650	14,170
ETH-87753(1)	MD13-3455G	382	foraminifera	13,538	38	14,800	15,510	15,180
ETH-87752*(1)	MD13-3455G	447	foraminifera	13,758	32	15,220	15,790	15,500
ETH-87751*(1)	MD13-3455G	472	foraminifera	14,566	38	16,330	16,970	16,650
ETH-87746	MD13-3459G	22	foraminifera	8585	26	8500	8970	8710
ETH-87747*	MD13-3459G	172	foraminifera	12,170	34	13,090	13,430	13,260
ETH-87748	MD13-3459G	422	foraminifera	12,838	31	13,730	14,140	13,930
ETH-87749*	MD13-3459G	552	foraminifera	12,948	32	13,800	14,300	14,050
ETH-87750*	MD13-3459G	742	foraminifera	14,413	39	16,140	16,760	16,420
ETH-87743	MD13-3462G	2	foraminifera	5777	25	5580	5920	5760
ETH-87744	MD13-3462G	37	foraminifera	22,811	78	25,970	26,530	26,220
ETH-103700	MD13-3462G	37	bryozoan	22,918	72	26,050	26,640	26,345

4.3. Grain size

Overall, $\bar{SS}$ varies between approximately 17 (core MD13-3455G) and 26 μm (core MD13-3462G). In core MD13-3462G, the transition from GS-3 to GI-1 is characterized by a decrease in $\bar{SS}$ from ~23 to ~21 μm (Fig. 3), though possibly as a result of low sampling resolution. Such a decrease in $\bar{SS}$ also characterizes the passage from GS-2.1 to GI-1 in core MD13-3455G (from ~21 to ~17 μm), despite such a trend not being noticeable in core MD13-3459G, possibly also due to a lack of GS-2.1 aged samples (Fig. 3). The Early GI-1 is marked by a gradual increase in $\bar{SS}$ in both MD13-3455G and MD13-3459G, respectively from ~17 to ~22 μm and from ~18 to ~22 μm (Fig. 3). Relatively high and stable $\bar{SS}$ values between ~20 and ~ 23 μm are recorded during Late GI-1 in core MD13-3459G (Fig. 3). The transition from GI-1 to the Holocene is characterized by a decrease in $\bar{SS}$ values in all three cores (from ~22.5 to ~21 μm, ~21 to ~19 μm and ~ 23.5 to ~20 μm in cores MD13-3462G, MD13-3455G and MD13-3459G respectively). These changes are mirrored by the mean grain size ($\bar{GS}$; Fig. 3). The paired Student *t*-test revealed that the observed $\bar{SS}$ differences between MD13-3455G and MD13-3459G during GI-1 are significant ($t = 14.96$, $p \leq 0.0001$; Fig. 5).

$\bar{SS}$ has been widely used as a proxy for bottom water current velocity (McCave and Hall, 2006). However, since coral framework can locally reduce bottom current speed and lead to the deposition of fine material, $\bar{SS}$ may be underestimated in the presence of coral cover, hence challenging the applicability of the $\bar{SS}$ proxy in CWC mound records (Huvenne et al., 2009; Eisele et al., 2011). In order to evaluate this potential bias, $\bar{SS}$ values were compared to coral abundances (vol%) obtained by quantitative analysis of CT scans (Fig. 6). In all three cores, there is no significant correlation between $\bar{SS}$ and coral abundance (Fig. 6), hence indicating that the variation in $\bar{SS}$ in these cores is not solely related to coral abundance but that other environmental parameters, such as local hydrography and regional oceanography, play a role.

End-member modelling performed on all three cores identified 5 robust end-members (Fig. 7). The two end-members (EM) that explain the most the observed variance are EM2 (31%) and EM3 (58%), which have respectively a mode of 3.9 φ (i.e. 68 μm) and 5.5 φ (i.e. 22 μm) (Fig. 7). The remaining 11% of the total variance is shared between EM1 (mode of 1.8 φ, i.e. 300 μm), EM4 (mode of 7.8 φ, i.e. 4.6 μm), and EM5 (mode of 8.5 φ, i.e. 2.8 μm) (Fig. 7). EM2 associated with EM5 is characteristic of the base of Early GI-1 (14.69 to 14.05 ka), whilst the later Early GI-1 and Late GI-1 (14.05 to 11.27) are dominated by EM3 (Fig. 3). This shift in End-members matches the $\bar{SS}$ and $\bar{GS}$ records (Fig. 3). The Holocene, noticeably the Mid and Late Holocene, is in contrast characterized by the dominance of EM2 and to a lesser extent EM1 and EM5 in cores MD13-3462G and MD13-3455G (Fig. 3).

5. Discussion

5.1. Age offsets: signs of reworked foraminifera and stagnating coral reefs?

Hiatuses and age reversals are regularly observed in CWC mounds (e.g. Dorschel et al., 2005; Kano et al., 2007; Frank et al., 2009; López Correa et al., 2012; Raddatz et al., 2014; Stalder et al., 2018). However, as explicited in section 4.1, split-core and CT-scan investigations together with grain size analyses (Fig. 3) did not allow to identify any erosive and/or gravitational-induced sedimentary features in either of the cores. The absence of coral age reversals implies that the recovered mound sediments did not experience periods of mound collapse/toppling or transport and can be confidently used to reconstruct mound build-up along BRI. Yet, there exists an offset between radiocarbon benthic foraminiferal and U-series coral ages within certain depth intervals (Fig. 3). These offsets may be defined as positive (i.e. benthic foraminiferal age younger than coral age) or negative (i.e. benthic foraminiferal age older than coral age). For example, at 382 cm depth in core MD13-3455G, benthic foraminifera yielded an age ~ 430 years older than the coral fragment dated 64 cm below it (Fig. 3). Such negative offsets occur during GI-1 (Fig. 3), whilst in contrast, the Holocene is characterized by positive offsets between benthic foraminiferal and coral ages (e.g. at respectively 2 and 22 cm depth in cores MD13-3462G and MD13-3459G, benthic foraminifera are ~950 and ~ 510 years younger than the coral fragments dated respectively 4 and 1 cm above them). The offset between coral U—Th is hence inconsistent with benthic ^{14}C foraminiferal ages and could reflect reworking/transport of benthic foraminifera and/or corals or variations in seawater δ^{234}U and/or local ^{14}C reservoir ages. There is indeed evidence that seawater δ^{234}U varies over interglacial-glacial cycles (Robinson et al., 2004; Esat and Yokoyama, 2006; Chen et al., 2016), noticeably in the Mediterranean Sea (Krengel, 2020), and that the ^{14}C reservoir age in the Mediterranean Sea varied during the last 16 kyr (Siani et al., 2001). At the EMCP, Krengel (2020) noticed an increase in δ^{234}U values from 28 ka (143 ‰) to 15 ka (148 ‰), whereas the δ^{234}U record did not vary considerably during the last 16 kyr (149–150 ‰). These observations suggest that variations in seawater δ^{234} over the last 16 kyr are probably not the cause for the observed offset between coral U—Th and benthic ^{14}C foraminiferal ages. In contrast, whilst Mediterranean ^{14}C reservoir ages were stable during the Holocene (390 ± 80 yr), they increased during GI-1 and even more so during GS-2.1 (810 ± 130 yr at 15.7 kyr) (Siani et al., 2001). Such variations in ^{14}C reservoir ages could lead to the offset observed between coral U—Th and benthic ^{14}C foraminiferal ages during GS-2.1 and GI-1 (Fig. 3). However, varying ^{14}C reservoir ages cannot explain both the observed negative and positive offsets. We propose that the discrepancies between coral U—Th and benthic ^{14}C foraminiferal ages may also reflect the allochthonous or autochthonous nature of

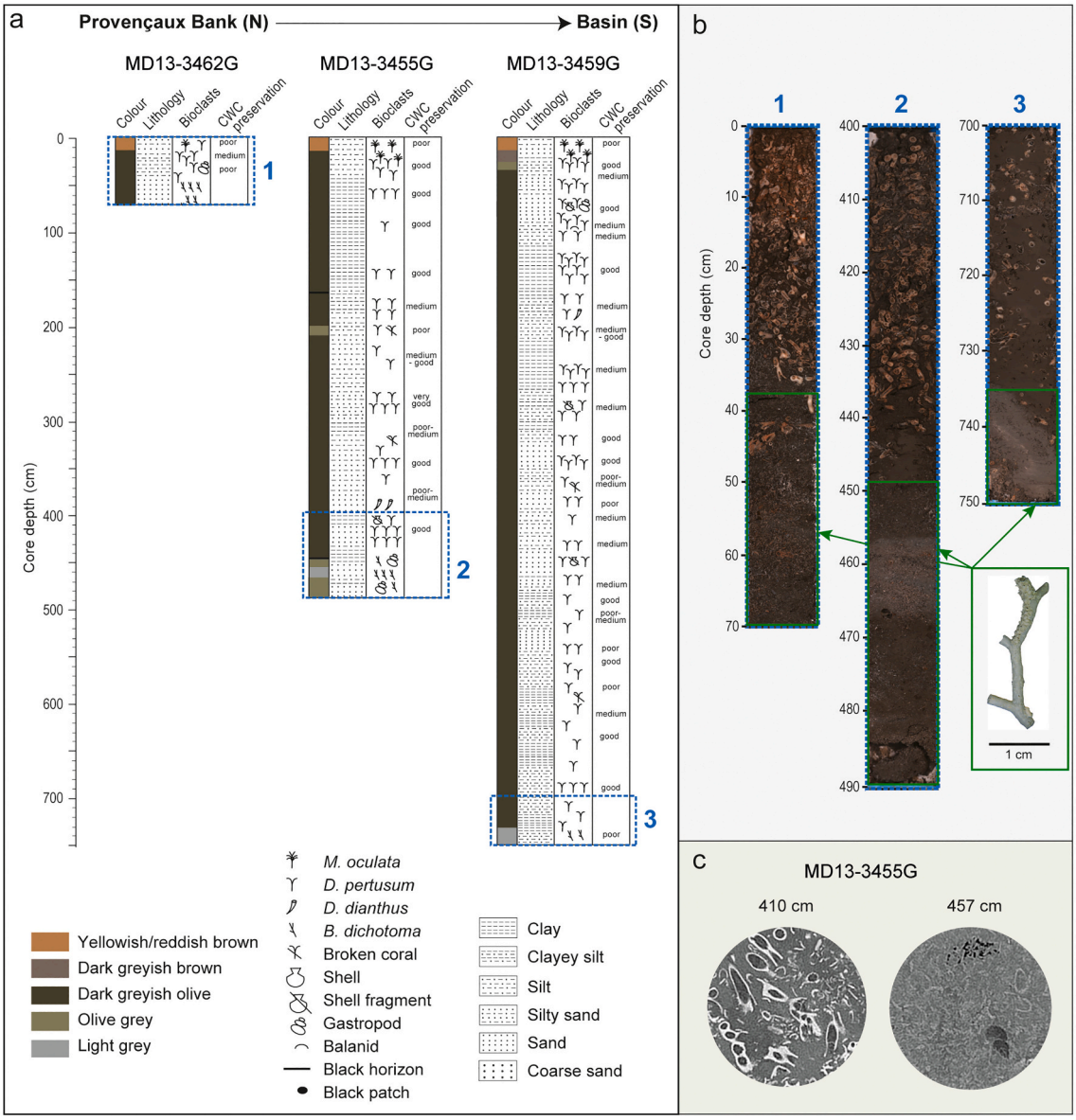

Fig. 2. (a) Stratigraphic description of cores MD13-3462G, MD13-3455G and MD13-3459G; (b) Split-core surface images of selected core sections (blue dashed rectangles) showing the transition from a bryozoan-dominated to a cold-water coral-dominated interval. *Buskea dichotoma*, the dominant species in the bryozoan-dominated intervals, is illustrated (green rectangle); (c) Computed tomography images from core MD13-3455G demonstrating the differences between coral-dominated (410 cm depth, left) and bryozoan-dominated (457 cm depth, right) layers. (For interpretation of the references to colour in this figure legend, the reader is referred to the web version of this article.)

benthic foraminifera contained within the coral framework and the timing of their development (contemporaneous or not with the corals), which would in turn be related to different phases of reef formation and thus changes in seafloor environmental conditions.

On the one hand, negative offsets could indicate the transport by strong bottom currents of older dead allochthonous benthic foraminifera from surrounding off-mound sediments. This phenomenon has previously been proposed to affect dead benthic foraminiferal assemblages at the surface of the Irish Moira Mounds (Fentimen et al., 2020b). The investigation of grain size distributions in on and off-mound settings by Wang et al. (2021) suggests that during times of mound formation at the EMCP, strong bottom currents caused a bypass or even erosion of fine sediment in off-mound areas, whereas this material could still be baffled by the coral framework and deposited on-mound, as evidenced by the modes of EM2 and EM3 (Figs. 3 and 7). These observations further strengthen the hypothesis that dead benthic foraminifera may be transported from surrounding settings and deposited within the coral framework during periods of reef development at BRI. The high mound aggradation rates recorded during GI-1 (Fig. 4), which is the time period when negative age offsets occur, would corroborate this assumption. On the other hand, during the Holocene, when positive offsets are observed, the low mound aggradation rates and the diminishing $\bar{S}S$ values imply that bottom currents were weaker, thus favouring mound stagnation (Fig. 3). These seafloor conditions would have prevented erosion and transport of dead benthic foraminifera, whilst living autochthonous benthic foraminifera would have colonized the exposed older dead coral framework and sediments. The offsets between coral and foraminiferal ages would hence reflect the different phases of coral reef development and sediment infilling of the coral framework. Overall, our observations demonstrate that transport and deposition of allochthonous foraminifera within the coral framework, together with variations in seawater $\delta^{234}U$ and ^{14}C reservoir ages, need to all be considered when

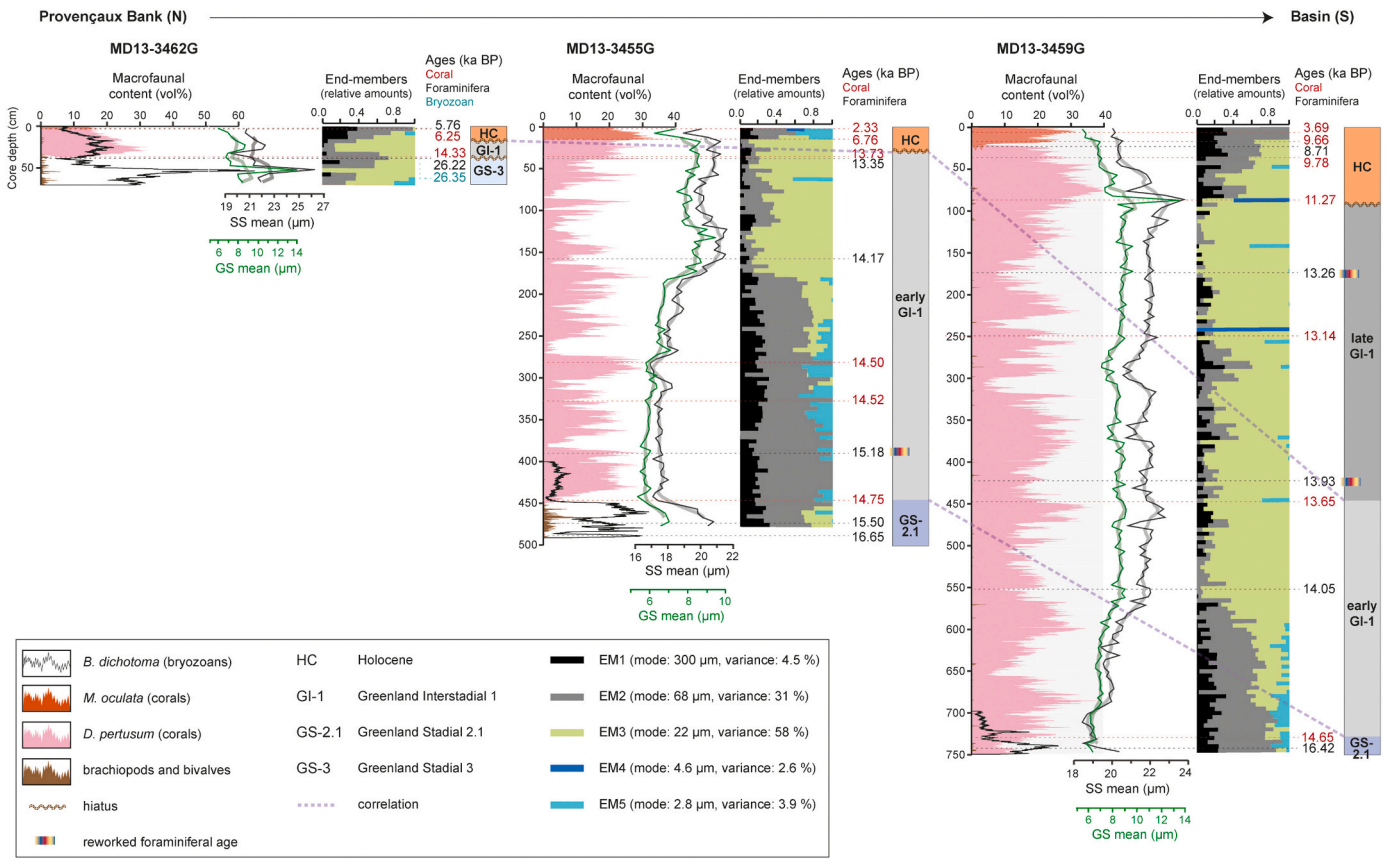

Fig. 3. Stratigraphic correlation between cores MD13-3462G, MD13-3455G and MD13-3459G. Displayed are the radiocarbon foraminiferal ages and the Uranium-series cold-water coral ages (ka BP), macrofaunal abundance (see legend), sortable silt (SS) mean grain size (black curve), mean grain size (siliciclastic fraction; green curve), grain-size end-members, and the stratigraphy. The bold shaded curves represent the running mean (with **n = 3**) for SS mean and GS mean. The distinction between different episodes of Greenland Interstadial 1 (Early vs. Late GI-1) is based on the U-series coral ages. (For interpretation of the references to colour in this figure legend, the reader is referred to the web version of this article.)

constructing the stratigraphic framework of CWC mounds.

5.2. Staggered mound build-up along Brittlestar Ridge I

5.2.1. Greenland Stadials 2.1 and 3

Benthic foraminiferal aggradation rates during GS-2.1 are low along Brittlestar Ridge I (Fig. 4). Corals are absent or scarcely distributed, matching the observations made by McCulloch et al. (2010) who noticed an absence of Last Glacial Maximum dated coral samples in the Mediterranean, which the authors attributed to a decline of coral communities due to unvafourable environmental conditions. However, recent studies have added nuances to these conclusions, with evidence of a sustained development of CWCs during the Last Glacial Maximum off the coast of Tunisia (Corbera et al., 2022), contrasting with an absence or extreme scarceness of CWC development during GS-2.1 at BRI and within the CMP (Corbera et al., 2021; Fentimen et al., 2022; Wienberg et al., 2022).

The high abundance of the erect cheleistome bryozoan species *B. dichotoma* during both GS-3 and GS-2.1 is a striking feature in all three cores (Fig. 3). Such densely-packed bryozoan intervals have not been previously reported in CWC mounds from the Mediterranean Sea nor from Atlantic counterparts, though *B. dichotoma* has been described in association with *M. oculata* between 180 and 350 m depth in the Blanes Canyon (northern Balearic Sea; Zabala et al., 1993), whilst Stalder et al. (2015) documented abundant *B. dichotoma* as subordinate components of *M. oculata/D. pertusum* communities in the Alboran Sea. They are indeed usually associated to corals as binders and encrusters (Matsuyama et al., 2015; Stalder et al., 2015). The occurrence of cm-thick bryozoan-dominated intervals almost entirely consisting of *B. dichotoma* is thus uncommon. Entire colonies were not detected at BRI, but the presence of large, unworn branch fragments including basal portions of colonies, points to an in situ production and thus, negligible displacement.

Only a few bryozoan species in the Mediterranean are known as habitat-forming and framework-builders (Lombardi et al., 2014). As elsewhere in the world, bryozoan bioconstructions from the Mediterranean are known from areas located above the shelf-break (Wood et al., 2012). A dozen species (including the erect branching *Pentapora* spp., *Smittina cervicornis*, *Adeonella* spp., *Schizoretepora serratimargo* and *Myriapora truncata* as well as some multilaminar encrusters) have been reported, with *Pentapora fascialis* forming relevant densities, each growing up to 60 cm in diameter and 1 m in height (Lombardi et al., 2014). Although it thrives in this basin, *B. dichotoma* has never been reported to form bioconstructions or being associated to other bryozoan frame-builders in the Mediterranean Sea or elsewhere (Taylor and Allison, 1998; Weedon and Taylor, 2008; Wood et al., 2012; Hageman et al., 2015; Rosso and Di Martino, 2016). This species frequently occurs in deep shelf (>60 m depth) to upper slope habitats, where populations consist of sparse colonies (Rosso and Di Geronimo, 1998; Madurell et al., 2013) and are rarely found within fossil bryozoan associations (Rosso, 2005). Fink et al. (2013) calculated low GS-2.1 sedimentation rates (11 cm kyr^{-1}) in an off-mound setting adjacent to BRI. In contrast to these off-mound sedimentation rates, the GS-2.1 MAR_F (22 and 80 cm kyr^{-1}, respectively for MD13-3455G and MD13-3459G; Fig. 4) indicate that sedimentation rates were on average two to eight-fold higher on-mound than off-mound. These observations suggest that sediment input was

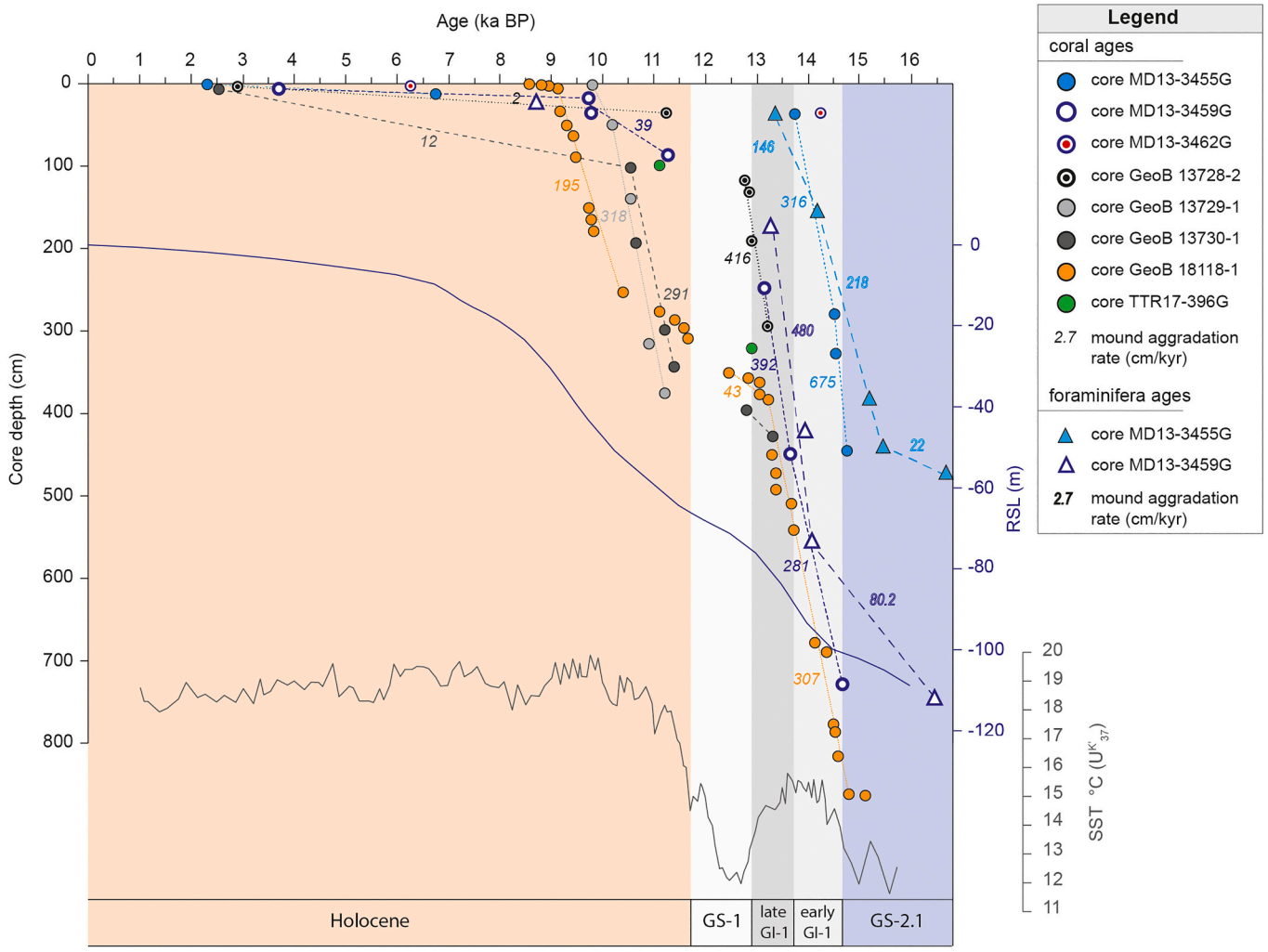

Fig. 4. Mound aggradation rates calculated from U-series coral ages (circles) and radiocarbon benthic foraminiferal ages (triangles) for Brittlestar Ridge I compiled from cores MD13-3455G (Fentimen et al., 2020a), MD13-3459G (this study), MD13-3462G (this study), GeoB 13,728–2, GeoB 13,729–1, GeoB 13,730–1 (Fink et al., 2013) and TTR17-396G (Stalder et al., 2018). Purple curve: Relative Sea Level (recorded in southern Sardinia) according to Lambeck et al. (2011). Black curve: Sea Surface Temperature (SST) reconstruction for the central Alboran Sea (core MD95–2043; 36°8.6′N; 2°37.3′W; Cacho et al., 2002). GS-1: Greenland Stadial 1, GI-1: Greenland Interstadial 1, GS-2.1: Greenland Stadial 2.1. (For interpretation of the references to colour in this figure legend, the reader is referred to the web version of this article.)

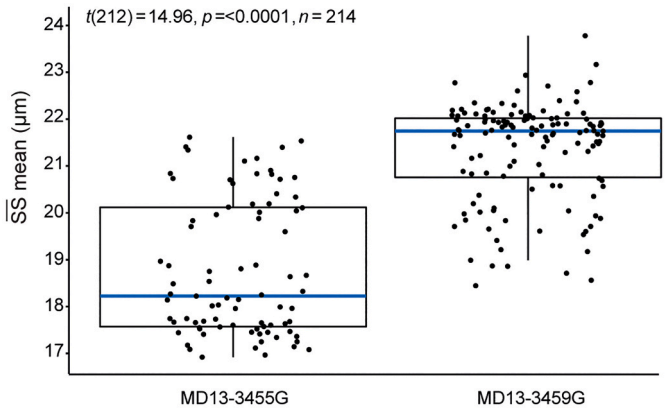

Fig. 5. Paired Student *t*-test comparing sortable silt mean grain size ($\overline{SS}$; µm) distributions from cores MD13-3455G and MD133459G for the Greenland Interstadial 1 (GI-1, 14.69 to 13.10 ka) period.

more important on the crest of BRI than in off-mound areas during GS-2.1 and/or that the *B. dichotoma* framework baffled inflowing sediment by slowing down bottom currents, in a similar way as scleractinian corals do. These observations would indicate that *B. dichotoma* communities play an active role in mound build-up during GS-2.1 along BRI.

5.2.2. *Greenland Interstadial 1*

The transition from GS-2.1 to GI-1 is marked by the development of *D. pertusum* colonies along BRI (Fig. 3). According to coral ages from each of the cores, the onset of coral growth took place between 14.75 and 14.33 ka BP along BRI (Table 2; Figs. 3 and 4; Fentimen et al., 2020a). This places the first post-GS-2.1 occurrence of *D. pertusum* in the two most southern cores (MD13-3459G and MD13-3455G) at the very beginning of GI-1 (Fig. 4). This timing matches previous observations made by Wienberg (2019) in the Alboran Sea and Wienberg et al. (2022) at BRI, which place the deglacial start-up of coral mound development at respectively ~14.60 and ~ 15.10 ka BP, similar to the onset of coral development in the WMCP and South CMP during GI-1 (14.1 and 14.5 ka BP respectively; Wang et al., 2019; Corbera et al., 2021). MAR_C at the beginning of GI-1 are maximal and reach 675 cm kyr^{-1} (Fig. 4), hence confirming that CWC colonization experienced a rapid start-up phase at

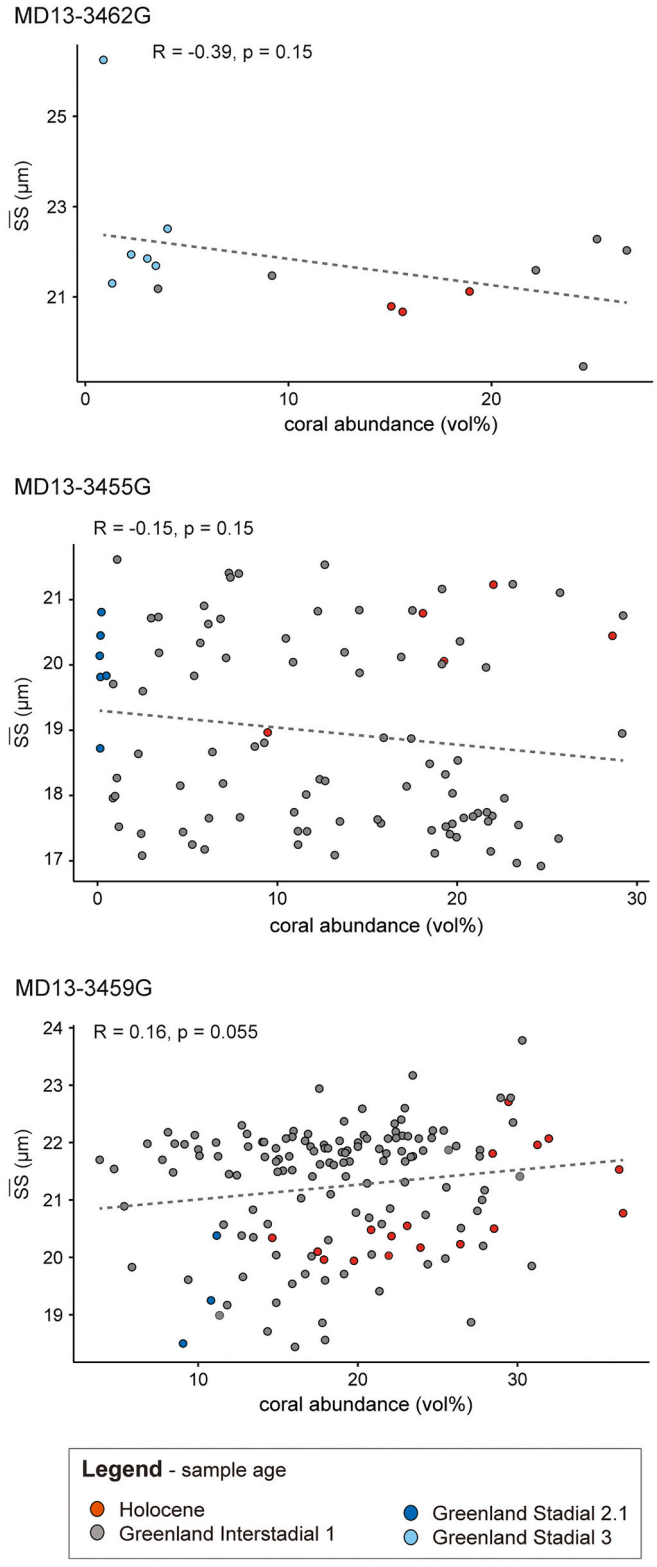

Fig. 6. Sortable silt mean grain size ($\overline{SS}$; μm; i.e. the arithmetic mean of the 10–63 μm size fraction) vs. coral abundance (vol%) for cores MD13-3462G, MD13-3455G and MD13-3459G.

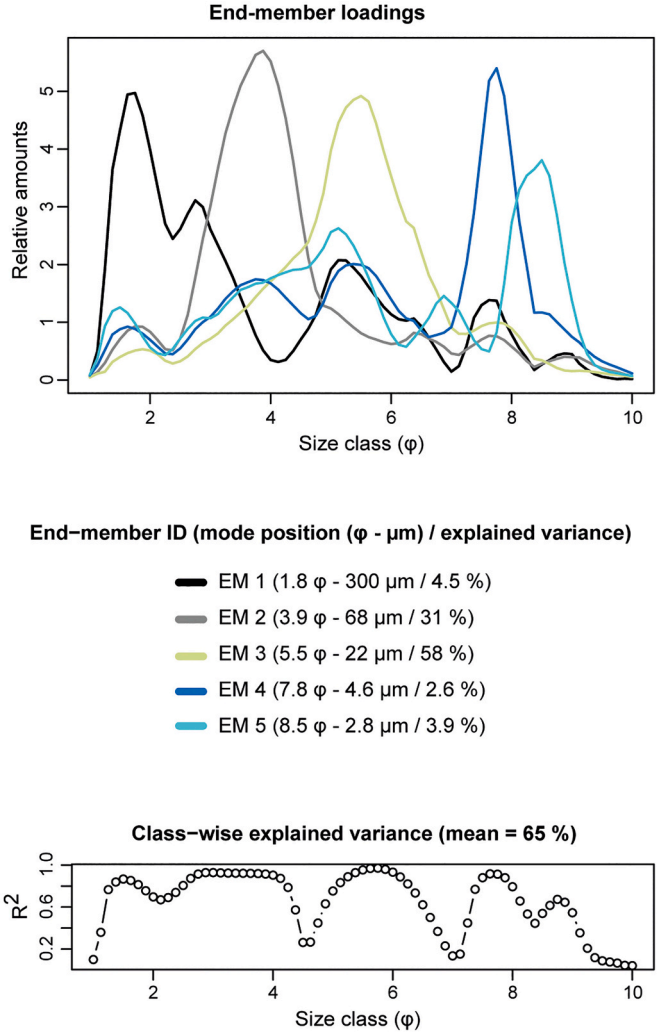

Fig. 7. Grain size end-member loadings, ID (mode position and explained variance), and class-wise explained variance.

BRI, as suggested by Fink et al. (2013) and Titschack et al. (2016). MAR_C range between ~281 and ~ 392 cm kyr^{-1} and match previous values calculated for cores GeoB 13,728–2 (~416 cm kyr^{-1}; Fig. 4; Fink et al., 2013) and GeoB 18,118–1 (~307 cm kyr^{-1}; Fig. 4; Wienberg et al., 2022), whilst being overall higher than rates reported for GI-1 at the CMP (44–91 cm kyr^{-1}; Corbera et al., 2021) and at the WMCP (178 cm kyr^{-1}; Wang et al., 2019). MAR_F at BRI are also high during the Early GI-1, noticeably at the most southern part (480 cm kyr^{-1}; MD13-3459G; Fig. 4). Overall, all the available data points to a rapid start-up of coral colonization at BRI at the very beginning of GI-1 (Fig. 4).

Although the GI-1 onset of CWC colonization has a similar age in all cores from the crest of BRI (Fig. 4), mound build-up during GI-1 is uneven and follows a different pattern along BRI (Figs. 3 and 8). Mound build-up during GI-1 is extremely limited in the northernmost area of BRI (MD13-3462G) with only ~15 cm of deposits (Figs. 3 and 8). In contrast, it is noticeably higher at the centre of BRI (~420 cm of deposits in MD13-3455G), and even greater in the southern area of BRI (~650 cm of deposits in MD13-3459G) (Figs. 2 and 3). This trend is generally confirmed by other cores taken from BRI, with respectively ~200 cm and ~ 500 cm of GI-1 deposits in the northern TTR17-396G and southernmost GeoB 18,118–1, though cores GeoB 13,728–2 and GeoB 13,730–1 located between MD13-3455G and MD13-3459G demonstrate respectively ~300 and ~ 90 cm of Late GI-1 deposits (Fig. 8). During the Early GI-1, mound build-up was more important in core MD13-3455G (central area) than in all other cores (Fig. 8), whereas Late GI-1 build-up is greatest in cores MD13-3459G (northern area) and GeoB 13,728–2 (central area) (Fig. 8). In addition to this spatial heterogeneity, a temporal heterogeneity also characterizes mound build-up along BRI during GI-1. Mound build-up shows a staggered pattern: it is restricted to the Early GI-1 in MD13-3455G (central area of BRI), whilst in MD13-3459G

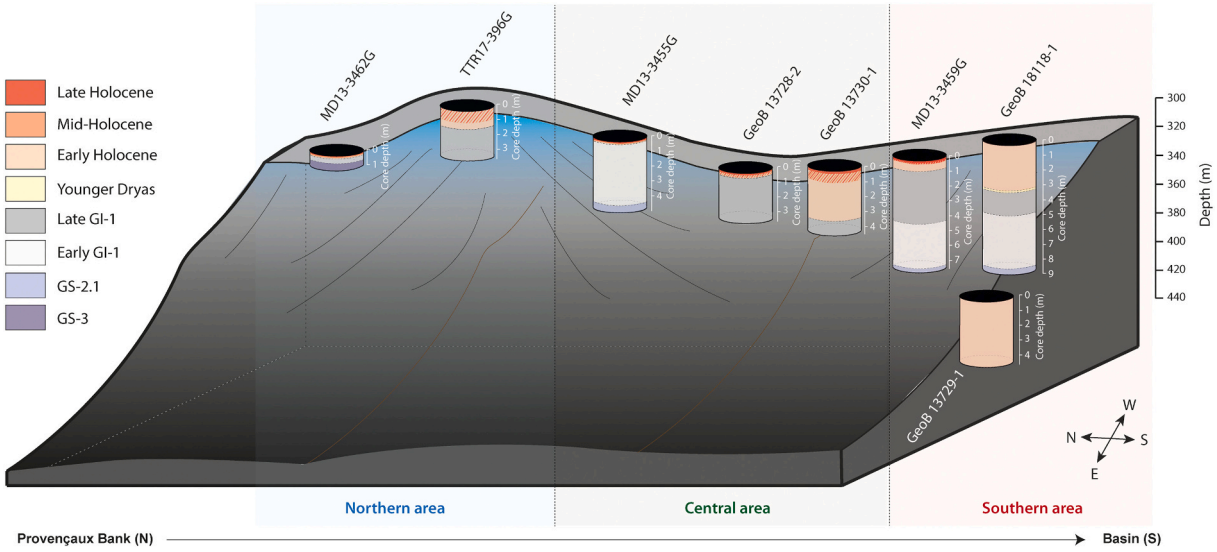

Fig. 8. Sketch illustrating the temporal distribution and variability of mound build-up at Brittlestar Ridge I as implied by core records MD13-3462G, MD13-3455G and MD133459G (this study), TTR17-396G (Stalder et al., 2018), GeoB 13,728–2, GeoB 13,730–1 and GeoB 13,729–1 (Fink et al., 2013), and GeoB 18,118–1 (Wienberg et al., 2022). Cores are not to scale with the illustration of the ridge. The limits between the different time periods are based on all available coral and foraminiferal ages, and are hence subject to uncertainties inherent to the stratigraphy of each individual core. The limits between the northern, central, and southern area are indicative and intended to facilitate the understanding of the text. See Fig. 1c for the location of the cores.

(southern area of BRI) vertical aggradation took place during both the Early and Late GI-1 (Figs. 3, 4 and 8). The occurrence of both Early and Late GI-1 mound deposits in the southern area is confirmed by core GeoB18118–1 (Fig. 8). In contrast to MD13-3455G, other cores from the central and northern areas of BRI only contain Late GI-1 deposits, although this is quite possibly due to the shortness of the cores (Fig. 8). This strong variability in mound development during GI-1, both spatial and temporal, implies that coral communities faced contrasting environmental conditions along the crest of BRI, and that at a very local scale, coral colonization and mound formation was highly variable (Fig. 8).

Corbera et al. (2021) highlighted the important differences in mound build-up between the northern (313 m water depth) and southern (417 m water depth) CMP during the Holocene. The authors suggest that these discrepancies may be linked to the vertical distance between the mounds' summits to the MAW/LIW interface. The internal waves formed at the interface between the two water masses may break when encountering a physical obstacle such as a slope or a mound (Pomar et al., 2012). These internal waves enhance lateral food availability and the delivery of sediments to CWC framework, and have been suggested to promote past and present CWC mound formation (Frederiksen et al., 1992; White et al., 2005; Thiem et al., 2006; White, 2007; Mienis et al., 2009; Mohn et al., 2014; Raddatz et al., 2014; Lim et al., 2018), such as in the WMCP (Wang et al., 2019). At the CMP, the shoaling of the MAW/LIW interface during the Holocene sea-level rise would have resulted in reduced food supply at the deeper southern mound, whilst not affecting the northern mound (Corbera et al., 2021). A similar relationship between mound formation and a shifting water mass interface has been described in detail at the Belgica Mound Province (Porcupine Seabight, NE Atlantic; Wienberg et al., 2020). During the Holocene, the upward shift of the Eastern North Atlantic Water/MOW transition zone would have led to a reactivation of mound formation first at ~950 m at ~11.3 ka BP and about 2.7 ky later at ~700 m water depth (at ~8.6 ka BP; Wienberg et al., 2020). The Mauritanian Coral Mound Province also shows a depth-related millennial-scale variation in mound formation, where mound development stopped much earlier in shallower waters (415 m) than in deeper parts (490 m), possibly as a result of vertical changes in the arrangement of intermediate water masses (Wienberg et al., 2018). Along BRI, all considered cores (except core GeoB 13,729–1) are all situated at approximately the same water depth (±42 m; Table 1), <1 km apart from each other, and on the crest of BRI (Fig. 1c). Therefore, a depth-related variation in mound development during GI-1 along BRI, such as in the CMP or in the Mauritanian Coral Mound Province, is unlikely. Indeed, a shoaling or deepening of the MAW/LIW transition zone would have very probably affected all sites and cannot explain the observed GI-1 variability and staggered pattern in mound formation. Wagner et al. (2011) and De Clippele et al. (2018) demonstrated how local hydrodynamic regimes affect coral development at Tisler CWC Reef (Hvaler area, Norway). A sill separates Tisler Reef between a deeper SE side (~130 m) and a slightly shallower NW side (~110 m; De Clippele et al., 2018). Although CWC growth takes place on both sides of the sill, Wagner et al. (2011) and De Clippele et al. (2018) noticed that coral cover was significantly lower on the shallower NW side. The lower availability of hard substrates on the NW side, essential for the settlement of coral larvae, and the predominance of a SE-orientated current in the area would favour coral development on the SE side (De Clippele et al., 2018). This dominant current direction would result in enhanced downwelling of chlorophyll-rich water to the SE side. A close relationship between local hydrodynamic regimes and coral growth is also observed in other CWC reef provinces, such as at the Mingulay Reef Complex between 120 and 190 m depth (Western Scotland; Duineveld et al., 2012; Henry et al., 2013; Navas et al., 2014) and at the downslope Moira Mounds (~950 m; Lim et al., 2018). Similar local hydrodynamic processes may explain the heterogeneous coral mound formation during GI-1 along BRI. A moat surrounding the southern tip of BRI suggests that strong bottom-currents sweep the base of the ridge in this area (Fig. 1c). This observation may imply that the southern area, located nearer the tip of the ridge, benefits from enhanced bottom-current regimes and as such from a higher food and sediment supply, as opposed to the most northern site situated near the Banc des Provençaux. Moreover, average $\bar{SS}$ values are higher during the Early GI-1 in the southern area (core MD13-3459G) than in the central area of the ridge (core MD13-3455G; Figs. 3 and 6), thus further suggesting that bottom-currents were likely more vigorous here than in the central and northern areas. Such hydrodynamic conditions could have led to the greater development of coral mounds in the southern part of BRI during GI-1, confirming the recent conclusion drawn by Wang et al. (2021) that bottom current-related transport and baffling of suspended

sediments by coral framework is the key process promoting mound build-up at the EMCP. However, the observed differences in mound build-up cannot solely be explained by stronger current velocities in the southern area. Indeed, Early GI-1 aggradation is the most important in the central area (core MD13-3455G, Fig. 8), whilst other cores in the central and northern areas (GeoB 13,728–2 and TTR17-396G) show extensive Late GI-1 mound build-up (Fig. 8). These observations would indicate that the differences in mound aggradation at BRI cannot simply be boiled down to a north-south orientated bottom current velocity gradient. Indeed, other actors such as space colony growth constraints, substrate availability, and competition for food have a direct influence on coral distribution and also play a key role (Zibrowius, 1980, 1984; Freiwald et al., 1997). For example, Corbera et al. (2019) studied the megafaunal distribution at the surface of the CMP and highlighted that colony size and CWC density increased with proximity to the mounds' summits. Given the position of core MD13-3462G, it is possibly situated within an inter-mound area off the summit, hence explaining the very limited build-up during the last 26 kyr (Fig. 8). Overall, although the data at hand does not allow us to fully illucidate the actors behind the staggered mound aggradation along BRI, our observations show the intricacies of coral mound build-up within a limited space and time.

5.2.3. Greenland Stadial 1 and the Holocene

Our results suggest that coral occurrences along BRI are limited to the transition period between GI-1 and GS-1, thereby confirming previous observations made by Fink et al. (2015) and Stalder et al. (2018) (Figs. 3 and 4). The absence of corals during GS-1 has also been noted in other parts of the Alboran Sea, e.g. at the WMCP (Wang et al., 2019) and at the CMP (Corbera et al., 2021). Several authors proposed that this hiatus in coral mound build-up is linked to a change in the Alboran Sea water mass circulation and an intensification of LIW currents (Fink et al., 2015; Wang et al., 2019; Corbera et al., 2021). However, these regional observations on coral mounds contradict a clear abundance peak of coral ages, including ages of framework forming species, during GS-1 in other regions of the Mediterranean Sea (McCulloch et al., 2010). This would confirm that the absence of coral mound build-up during GS-1 in the Alboran Sea is a regional specificity, as suggested by Wang et al. (2019). The Early Holocene marks the re-establishment of mound formation along BRI (Figs. 2 and 3), confirming previous observations made at the EMCP, WMCP and CMP (Fink et al., 2013, 2015; Stalder et al., 2015, 2018; Wang et al., 2019; Fentimen et al., 2020a; Corbera et al., 2021).

Mound build-up during the Early Holocene at the three studied core locations was considerably less important than during GI-1 (Fig. 4), with aggradation rates never exceeding ~40 cm kyr^{-1} (MD13-3459G; Fig. 4) and a near-complete absence of Holocene deposits in the central and northern cores (Figs. 3 and 8). Similar low aggradation rates were calculated for the Early Holocene by Corbera et al. (2021) in the southern CMP (24 cm kyr^{-1}). However, other cores sampled on BRI (GeoB 13,730–1, GeoB 18,118–1 and GeoB 13,729–1) demonstrate that other parts of BRI experienced an important phase of aggradation during the Early Holocene, with rates reaching 318 cm kyr^{-1} on the southern part of the slope (Figs. 4 and 8; Fink et al., 2013). An Early Holocene mound build-up episode is also observed at the WMCP and CMP, where aggradation rates reach respectively ~75–110 cm kyr^{-1} and ~ 200 cm kyr^{-1} (Wang et al., 2019; Corbera et al., 2021). At BRI, Early Holocene mound build-up appears to be concentrated in the southern area, although core MD13-3459G (located within the southern area) shows little Early Holocene deposits (Fig. 8). The overall greater aggradation in the southern area during the Early Holocene may be driven by increased bottom currents, as suggested by the higher average $\bar{S}S$ values (Fig. 3), though other drivers (e.g. substrate and food availability, competition) are to be considered (see section 5.2.2). Mound build-up at BRI during the Mid and Late Holocene is extremely reduced in most parts, although cores TTR17-396G and GeoB 13,730–1 (northern and central areas) hold ~100 cm of Mid and Late Holocene deposits (Fig. 8), again underlining the patchiness of mound development at BRI. The relative lack of aggradation during the Mid and Late Holocene is possibly a result of a progressive weakening of bottom currents throughout the last 11 kyr, as evidenced by a moderate decrease in $\bar{S}S$ values in the southern core (Fig. 3), and the establishment of unfavourable conditions during Sapropel S1. This possibly led to a retreat in coral population density and the change in coral dominance from *D. pertusum* to *M. oculata* during the Mid Holocene, as attested by the present-day scarcity of coral communities at BRI (Hebbeln, 2019).

6. Conclusion

The combined study of three novel and five previously investigated cold-water coral cores located along the crest of Brittlestar Ridge I (East Melilla Coral Province, Southeast Alboran Sea) points to an important spatial and temporal heterogeneity in mound build-up during the last 16 kyr. More favourable environmental conditions, noticeably stronger bottom currents, would have resulted in an overall greater coral mound build-up in the central and southern areas. However, coral mound build-up does not show a clear trend but rather a patchy temporal and spatial distribution along the ridge, suggesting that a number of other ecological actors (e.g. space constraints, substrate availability, competition) also have a key influence. This staggered coral mound build-up during the last 16 kyr would reflect the patchiness of coral distribution and variability of macrohabitats, which is commonly observable on modern cold-water coral reefs. These observations prove that coral mound formation may show important discrepancies within a restricted geographical area, thus implying that mound build-up is not only governed by widespread climate variability but also by environmental changes at a much more local scale and during short (millennial to centennial) time intervals. Overall, this study highlights the differences in coral mound build-up within a restricted area, thereby stressing the importance of studying multiple and precisely located records of the same mound.

Sample availability

Archive halves of all core sections presented in this work are stored at the Department of Geosciences, University of Fribourg (Switzerland).

CRediT authorship contribution statement

Robin Fentimen: Writing – original draft, Investigation, Conceptualization, Methodology. **Eline J. Feenstra:** Writing – original draft, Investigation, Conceptualization, Methodology. **Andres Rüggeberg:** Writing – review & editing, Conceptualization. **Efraim Hall:** Investigation. **Antonietta Rosso:** Investigation. **Irka Hajdas:** Investigation. **David Jaramillo-Vogel:** Investigation. **Bernard Grobéty:** Investigation, Methodology. **Thierry Adatte:** Methodology. **David Van Rooij:** Investigation. **Norbert Frank:** Investigation. **Anneleen Foubert:** Writing – review & editing, Conceptualization, Methodology, Funding acquisition.

Declaration of Competing Interest

The authors declare that they have no competing interests.

Data availability

All datasets presented in this work are available at the open-access repository PANGEA (https://doi.pangaea.de/10.1594/PANGAEA.940743).

Acknowledgements

The authors would like to dedicate this manuscript to Prof. dr. Jean-Pierre Henriet, a key figure in mound research along the continental margins and initiator of the EuroFLEETS GATEWAYS project. We acknowledge the ship time provided by IPEV on R/V *Marion Dufresne II* within the framework of the EuroFLEETS GATEWAYS project (grant agreement 228344). We also would like to thank the lab technicians that provided critical support during sample preparation and measurements, namely Alexandre Salzmann and Christoph Neururer (University of Fribourg), Rene Eichstädter and Anne-Marie Wefing (University of Heidelberg) and Nicole Schwendener (Institute of Forensic Sciences at the University of Bern). We further thank the two anonymous reviewers who provided insightful and constructive comments and corrections to this work. The study has been funded through the SNF-projects (Swiss National Science Foundation) 4D-Diagenesis@Mound (SNF Project Number 200021_149247) and 200020_153125.

References

Addamo, A.M., Vertino, A., Stolarski, J., García-Jiménez, R., Taviani, M., Machordom, A., 2016. Merging scleractinian genera: the overwhelming genetic similarity between solitary *Desmophyllum* and colonial *Lophelia*. BMC Evol. Biol. 16, 108.

Ammar, A., Mauffret, A., Gorini, C., Jabour, H., 2007. The tectonic structure of the Alboran margin of Morocco. Rev. Soc. Geol. Esp. 20, 247–271.

Angeletti, L., Castellan, G., Montagna, P., Remia, A., Taviani, M., 2020. The "Corsica Channel Cold-Water Coral Province" (Mediterranean Sea). Front. Mar. Sci. 7.

Ausín, B., Flores, J.A., Sierro, F.J., Bárcena, M.A., Hernández-Almeida, I., Francés, G., Gutiérrez-Arnillas, E., Martrat, B., Grimalt, J.O., Cacho, I., 2015. Coccolithophore productivity and surface water dynamics in the Alboran Sea during the last 25 kyr. Palaeogeogr. Palaeoclimatol. Palaeoecol. 418, 126–140.

Bárcena, M.A., Cacho, I., Abrantes, F., Sierro, F.J., Grimalt, Flores, J.A., 2001. Paleoproductivity variations related to climatic conditions in the Alboran Sea (western Mediterranean) during the last glacial–interglacial transition: the diatom record. Palaeogeogr. Palaeoclimatol. Palaeoecol. 167, 337–357.

Cacho, I., Sierro, F., Shackleton, N.J., Elderfield, H., Grimalt, J., 2002. Reconstructing Alboran Sea hydrography during the last organic rich layer formation. Geochim. Cosmochim. Acta 66. A115.

Camafort, M., Gracia, E., Ranero, C.R., 2020. Quaternary Seismostratigraphy and tectonosedimentary evolution of the North Tunisian Continental margin. Tectonics 39.

Carlier, A., Le Guilloux, E., Olu, K., Sarrazin, J., Mastrototaro, F., Taviani, M., Clavier, J., 2009. Trophic relationships in a deep Mediterranean cold-water coral bank (Santa Maria di Leuca, Ionian Sea). Mar. Ecol. Prog. Ser. 397, 125–137.

Chen, T., Robinson, L.F., Beasley, M.P., Claxton, L.M., Andersen, M.B., Gregoire, L.J., Wadham, J., Fornari, D.J., Harpp, K.S., 2016. Ocean mixing and ice-sheet control of seawater 234U/238U during the last deglaciation. Science 354 (6312), 626–629.

Cheng, H., Edwards, R.L., Hoff, J., Gallup, C.D., Richards, D.A., Asmerom, Y., 2000. The half-lives of uranium-234 and thorium-230. Chem. Geol. 169, 17–33.

Comas, M.C., Pinheiro, L.M., 2007. Discovery of carbonate mounds in the Alboran Sea: the Melilla mound field. In: 1st International Conference of the Moroccan Association of Petroleum Geologists (MAPG) in Association with the American Association of Petroleum Geologists (AAPG), Marrakesh, October, pp. 28–31.

Comas, M.C., Platt, J.P., Soto, J.I., Watts, A.B., 1999. The origin and tectonic history of the Alboran Basin: Insights from Leg 161 results. In: Zahn, R., Comas, M.C., Klaus, A. (Eds.), Proceedings of the Ocean Drilling Program, Scientific Results, 161, pp. 555–580.

Corbera, G., Lo Iacono, C., Gràcia, E., Grinyo, J., Pierdomenico, M., Huvenne, V.A.I., Aguilar, R., Gili, J.M., 2019. Ecological characterisation of a Mediterranean cold-water coral reef: Cabliers Coral Mound Province (Alboran Sea, western Mediterranean). Prog. Oceanogr. 175, 245–262.

Corbera, C., Lo Iacono, C., Standish, D., Anagnostou, E., Titschack, J., Katsamenis, O., Cacho, I., Van Rooij, D., Huvenne, V.A.I., Foster, G.L., 2021. Glacio-eustatic variations and sapropel events as main controls on the Middle Pleistocene-Holocene evolution of the Cabliers Coral Mound Province (W Mediterranean). Quat. Sci. Rev. 253, 106783.

Corbera, G., Lo Iacono, C., Standish, C.D., Gràcia, E., Ranero, C., Huvenne, V.A.I., Anagnostou, E., Foster, G.L., 2022. Glacial-aged development of the Tunisian Coral Mound Province controlled by glacio-eustatic oscillations and changes in surface productivity. Mar. Geol. 446, 106772.

Davies, A.J., Guinotte, J.M., 2011. Global habitat suitability for framework-forming cold-water corals. PLoS One 6, e18483.

Davies, A.J., Wisshak, M., Orr, J.C., Roberts, J.M., 2008. Predicting suitable habitat for the cold-water coral *Lophelia pertusa* (Scleractinia). Deep-Sea Res. I Oceanogr. Res. Pap. 55, 1048–1062.

De Clippele, L.H., Huvenne, V.A.I., Orejas, C., Lundälv, T., Fox, A., Hennige, S.J., Roberts, J.M., 2018. The effect of local hydrodynamics on the spatial extent and morphology o cold-water coral habitats at Tisler Reef, Norway. Coral Reefs 37, 253–266.

De Mol, B., Van Rensbergen, P., Pillen, S., Van Herreweghe, K., Van Rooij, D., McDonnell, A., Huvenne, V.A.I., Ivanov, M., Swennen, R., Henriet, J.-P., 2002. Large deep-water coral banks in the Porcupine Basin, southwest of Ireland. Mar. Geol. 188, 193–231.

Dietze, M., Dietze, E., 2019. EMMAgeo: End-Member Modelling of Grain-size Data. R Package Version 0.9.7. https://CRAN.R-project.org/package=EMMAgeo.

Dorschel, B., Hebbeln, D., Rüggeberg, A., Dullo, W.-C., Freiwald, A., 2005. Growth and erosion of a cold-water coral covered carbonate mound in the Northeast Atlantic during the late Pleistocene and Holocene. Earth Planet. Sci. Lett. 233, 33–44.

Dorschel, B., Hebbeln, D., Foubert, A., White, M., Wheeler, A.J., 2007. Hydrodynamics and cold-water coral facies distribution related to recent sedimentary processes at Galway Mound west of Ireland. Mar. Geol. 244, 184–195.

Douville, E., Sallé, E., Frank, N., Eisele, M., Pons-Branchu, E., Ayrault, S., 2010. Rapid and accurate U–Th dating of ancient carbonates using inductively coupled plasma-quadrupole mass spectrometry. Chem. Geol. 272, 1–11.

Duineveld, G., Jeffreys, R., Lavaleye, M., Davies, A., Bergman, M., Watmough, T., Witbaard, R., 2012. Spatial and tidal variation in food supply to shallow cold-water coral reefs of the Mingulay Reef complex (Outer Hebrides, Scotland). Mar. Ecol. Prog. Ser. 444, 97–115.

Eisele, M., Frank, N., Wienberg, C., Hebbeln, D., López Correa, M., Douville, E., Freiwald, A., 2011. Productivity controlled cold-water coral growth periods during the last glacial off Mauritania. Mar. Geol. 280, 143–149.

Ercilla, G., Juan, C., Hernández-Molina, F.J., Bruno, M., Estrada, F., Alonso, B., Casas, D., Farran, M., Llave, E., García, M., Vázquez, J.T., D'acremont, E., Gorini, C., Palomino, D., Valencia, J., El Moumni, B., Ammar, A., 2016. Significance of bottom currents in deep-sea morphodynamics: an example from the Alboran Sea. Mar. Geol. 378, 157–170.

Esat, T.M., Yokoyama, Y., 2006. Variability in the uranium isotopic composition of the oceans over glacial-interglacial timescales. Geochim. Cosmochim. Acta 70, 4140–4150.

Fentimen, R., Feenstra, E.J., Rüggeberg, A., Vennemann, T., Hajdas, I., Adatte, T., Van Rooij, D., Foubert, A., 2020a. Cold-water coral mound archive provides unique insights into intermediate water mass dynamics in the Alboran Sea during the last deglaciation. Front. Mar. Sci. 7, 354.

Fentimen, R., Lim, A., Rüggeberg, A., Wheeler, A.J., Van Rooij, D., Foubert, A., 2020b. Impact of bottom water currents on benthic foraminiferal assemblages in a cold-water coral environment: the Moira Mounds (NE Atlantic). Mar. Micropaleontol. 154, 101799.

Fentimen, R., Feenstra, E.J., Rüggeberg, A., Hall, E., Rime, V., Vennemann, T., Hajdas, I., Rosso, A., Van Rooij, D., Adatte, T., Vogel, H., Frank, N., Foubert, A., 2022. A 300 000-year record of cold-water coral mound build-up at the East Melilla Coral Province (SE Alboran Sea, western Mediterranean). Clim. Past 18 (8), 1915–1945.

Fink, H.G., Wienberg, C., De Pol-Holz, R., Wintersteller, P., Hebbeln, D., 2013. Cold-water coral growth in the Alboran Sea related to high productivity during the late Pleistocene and Holocene. Mar. Geol. 339, 71–82.

Fink, H.G., Wienberg, C., De Pol-Holz, R., Hebbeln, D., 2015. Spatio-temporal distribution patterns of Mediterranean cold-water corals (*Lophelia pertusa* and *Madrepora oculata*) during the past 14,000 years. Deep-Sea Res. I Oceanogr. Res. Pap. 103, 37–48.

Flögel, S., Dullo, W.-C., Pfannkuche, O., Kiriakoulakis, K., Rüggeberg, A., 2014. Geochemical and physical constraints for the occurrence of living cold-water corals. Deep-Sea Reas. II 99, 19–26.

Foubert, A., Depreiter, D., Beck, T., Maignien, L., Pannemans, B., Frank, N., Blamart, D., Henriet, J.-P., 2008. Carbonate mounds in a mud volcano province off north-West Morocco: Key to processes and controls. Mar. Geol. 248, 74–96.

Frank, N., Paterne, M., Ayliffe, L., van Weering, T., Henriet, J.-P., Blamart, D., 2004. Eastern North Atlantic deep-sea corals: tracing upper intermediate water Δ14C during the Holocene. Earth Planet. Sci. Lett. 219, 297–309.

Frank, N., Ricard, E., Lutringer-Paquet, A., van der Land, C., Colin, C., Blamart, D., Foubert, A., Van Rooij, D., Henriet, J.-P., de Haas, H., van Weering, T., 2009. The Holocene occurrence of cold-water corals in the NE Atlantic: implications for coral carbonate mound evolution. Mar. Geol. 266, 129–142.

Frank, N., Freiwald, A., López Correa, M., Wienberg, C., Eisele, M., Hebbeln, D., Van Rooij, D., Henriet, J.-P., Colin, C., van Weering, T., de Haas, H., Buhl-Mortensen, P., Roberts, J.M., De Mol, B., Douville, E., Blamart, D., Hatté, C., 2011. Northeastern Atlantic cold-water coral reefs and climate. Geology 39, 743–746.

Frederiksen, R., Jensen, A., Westerberg, H., 1992. The distribution of the scleractinian coral *Lophelia pertusa* around the Faroe Islands and the relation to internal tidal mixing. Sarsia 77, 157–171.

Freiwald, A., 2002. Reef-forming cold-water corals. In: Wefer, G., Billet, D., Hebbeln, D., Jørgensen, B.B., Schlüter, M., Van Weering, T.C.E. (Eds.), Ocean Margin Systems. Springer, Berlin, Heidelberg, p. 495.

Freiwald, A., Henrich, R., Pätzold, J., 1997. Anatomy of a deep-water coral reef mound from Stjernsund, West-Finnmark, northern Norway. SEPM Spec. Publ. 56, 141–161.

Freiwald, A., Fosså, J.H., Grehan, A., Koslow, T., Roberts, J.M., 2004. In: Hain, S., Corcoran, E. (Eds.), Cold-Water Coral Reefs: Out of Sight - No Longer Out of Mind. UNEP_WCMC, Cambridge, UK, p. 86.

Freiwald, A., Beuck, L., Rüggeberg, A., Taviani, M., Hebbeln, D., 2009. The white coral community in the Central Mediterranean Sea revealed by ROV surveys. Oceanography 22, 58–74.

Hageman, S.J., Bock, P.E., Bone, Y., McGowran, B., 2015. Bryozoan growth habits: classification and analysis. J. Paleontol. 72, 418–436.

Hajdas, I., 2008. Radiocarbon dating and its applications in Quaternary studies. Eiszeitalter und Gegenwart Quat. Sci. J. 57, 24.

Hebbeln, D., 2019. Highly variable submarine landscapes in the alborán sea created by cold-water corals. In: Orejas, C., Jimenez, C. (Eds.), Mediterranean Cold-Water

Corals: Past, Present and Future: Understanding the Deep-Sea Realms of Coral. Springer International Publishing, p. 569.
Hebbeln, D., Wienberg, C., Wintersteller, P., Freiwald, A., Becker, M., Beuck, L., Dullo, C., Eberli, G.P., Glogowski, S., Matos, L., Forster, N., Reyes-Bonilla, H., Taviani, M., 2014. Environmental forcing of the Campeche cold-water coral province, southern Gulf of Mexico. Biogeosciences 11, 1799–1815.
Henry, L.A., Moreno Navas, J., Roberts, J.M., 2013. Multi-scale interactions between local hydrography, seabed topography, and community assembly on cold-water coral reefs. Biogeosciences 10, 2737–2746.
Hernández-Molina, F.J., Serra, N., Stow, D.A.V., Llave, E., Ercilla, G., Van Rooij, D., 2011. Along-slope oceanographic processes and sedimentary products around the Iberian margin. Geo-Mar. Lett. 31, 315–341.
Huvenne, V.A.I., Blondel, P., Henriet, J.-P., 2002. Textural analyses of sidescan sonar imagery from two mound provinces in the Porcupine Seabight. Mar. Geol. 189, 323–341.
Huvenne, V.A.I., De Mol, B., Henriet, J.-P., 2003. A 3D seismic study of the morphology and spatial distribution of buried coral banks in the Porcupine Basin, SW of Ireland. Mar. Geol. 198, 5–25.
Huvenne, V.A.I., Masson, D.G., Wheeler, A.J., 2009. Sediment dynamics of a sandy contourite: the sedimentary context of the Darwin cold-water coral mounds, Northern Rockall Trough. Int. J. Earth Sci. 98, 865–884.
Jaffey, A.H., Flynn, K.F., Glendenin, L.E., Bentley, W.C., Essling, A.M., 1971. Precision measurements of half-lives and specific activities of ^{235}U and ^{238}U. Phys. Rev. 4 (5), 1889–1906.
Jimenez-Espejo, F.J., Martinez-Ruiz, F., Rogerson, M., Gonzalez-Donoso, J.M., Romero, O.E., Linares, D., Sakamoto, T., Gallego-Torres, D., Rueda Ruiz, J.L., Ortega-Huertas, M., Perez Claros, J.A., 2008. Detrital input, productivity fluctuations, and water mass circulation in the westernmost Mediterranean Sea since the Last Glacial Maximum. Geochem. Geophys. Geosyst. 9, U11Q02. https://doi.org/10.1029/2008GC002096.
Jimenez-Espejo, F.J., Martinez-Ruiz, F., Sakamoto, T., Iijima, K., Gallego-Torres, D., Harada, N., 2007. Paleoenvironmental changes in the western Mediterranean since the last glacial maximum: High resolution multiproxy record from the Algero–Balearic basin. Palaeogeogr. Palaeoclimatol. Palaeoecol. 246, 292–306.
Juan, C., Ercilla, G., Hernández-Molina, F.J., Estrada, F., Alonso, B., Casas, D., García, M., Farran, M., Llave, E., Palomino, D., Vázquez, J.-T., Medialdea, T., Gorini, C., D'acremont, E., El Moumni, B., Ammar, A., 2016. Seismic evidence of current-controlled sedimentation in the Alboran Sea during the Pliocene and Quaternary: palaeoceanographic implication. Mar. Geol. 378, 292–311.
Kano, A., Ferdelman, T.G., Williams, T., Henriet, J.-P., Ishikawa, T., Kawagoe, N., Takashima, C., Kakizaki, Y., Abe, K., Sakai, S., Browning, E.L., Li, X., Integrated Ocean Drilling Program Expedition 307 Scientists, 2007. Age constraints on the origin and growth history of a deep-water coral mound in the Northeast Atlantic drilled during Integrated Ocean Drilling Program Expedition 307. Geology 35 (11), 1051–1054.
Krengel, T., 2020. 550,000 Years of Marine Climate Variability in the Western Mediterranean Sea Revealed by Cold-Water Corals. PhD thesis,. Heidelberg University (Germany), p. 189.
Lambeck, K., Antonioli, F., Anzidei, M., Ferranti, L., Leoni, G., Scicchitano, G., Silenzi, S., 2011. Sea level change along the Italian coast during the Holocene and projections for the future. Quat. Int. 232 (1–2), 250–257.
Lim, A., Huvenne, V.A.I., Vertino, A., Spezzaferri, S., Wheeler, A.J., 2018. New insights on coral mound development from groundtruthed high-resolution ROV-mounted multibeam imaging. Mar. Geol. 403, 225–237.
Lo Iacono, C., Gràcia, E., Ranero, C.E., Emelianov, M., Huvenne, V.A.I., Bartolomé, R., Booth-Rea, G., Prades, J., Ambroso, S., Dominguez, C., Grinyó, J., Rubio, E., Torrent, J., 2014. The West Melilla cold water coral mounds, Eastern Alboran Sea: Morphological characterization and environmental context. Deep-Sea Res. II Top. Stud. Oceanogr. 99, 316–326.
Lombardi, C., Taylor, P.D., Cocito, S., 2014. Bryozoan constructions in a changing Mediterranean Sea. In: Goffredo, S., Dubinsky, Z. (Eds.), The Mediterranean Sea: Its History and Present Challenges. Springer Netherlands, Dordrecht, p. 673.
López Correa, M., Montagna, P., Joseph, N., Rüggeberg, A., Fietzke, J., Flögel, S., Dorschel, B., Goldstein, S.L., Wheeler, A.J., Freiwald, A., 2012. Preboreal onset of cold-water coral growth beyond the Arctic Circle revealed by coupled radiocarbon and U-series dating and neodymium isotopes. Quat. Sci. Rev. 34, 24–43.
Madurell, T., Zabala, M., Dominguez-Carrió, C., Gili, J.M., 2013. Bryozoan faunal composition and community structure from the continental shelf off Cap de Creus (Northwestern Mediterranean). J. Sea Res. 83, 123–136.
Martínez-García, P., Comas, M., Soto, J.I., Lonergan, L., Watts, A.B., 2013. Strike-slip tectonics and basin inversion in the Western Mediterranean: the post-messinian evolution of the Alboran Sea. Basin Res. 25, 361–387.
Martorelli, E., Petroni, G., Chiocci, F.L., the Pantelleria Scientific Party, 2011. Contourites offshore Pantelleria Island (Sicily Channel, Mediterranean Sea): depositional, erosional and biogenic elements. Geo-Marine Lett. 31, 481–493.
Matos, L., Mienis, F., Wienberg, C., Frank, N., Kwiatkowski, C., Groeneveld, J., Thil, F., Abrantes, F., Cunha, M.R., Hebbeln, D., 2015. Interglacial occurrence of cold-water corals off Cape Lookout (NW Atlantic): first evidence of the Gulf Stream influence. Deep Sea Res. Part I 105, 158–170.
Matos, L., Wienberg, C., Titschack, J., Schmiedl, G., Frank, N., Abrantes, F., Cunha, M.R., Hebbeln, D., 2017. Coral mound development at the Campeche cold-water coral province, southern Gulf of Mexico: implications of Antarctic Intermediate Water increased influence during interglacials. Mar. Geol. 392, 53–65.
Matsuyama, K., Titschack, J., Baum, D., Freiwald, A., 2015. Two new species of erect Bryozoa (Gymnolaemata: Cheilostomata) and the application of non-destructive imaging methods for quantitative taxonomy. Zootaxa 4020, 81–100.
McCave, I.N., 2009. Nepheloid layers. In: Thorpe, S.A., Turekian, K.K. (Eds.), Encyclopedia of Ocean Sciences, Second edition. Academic Press, Oxford, pp. 8–18.
McCave, I.N., Hall, I.R., 2006. Size sorting in marine muds: processes, pitfalls, and prospects for paleoflow-speed proxies. Geochem. Geophys. Geosyst. 7, 1–37.
McCave, I.N., Manighetti, B., Robinson, S.G., 1995. Sortable silt and fine sediment size/composition slicing: parameters for palaeocurrent speed and palaeoceanography. Paleoceanography 10, 593–610.
McCulloch, M., Taviani, M., Montagna, P., López Correa, M., Remia, A., Mortimer, G., 2010. Proliferation and demise of deep-sea corals in the Mediterranean during the Younger Dryas. Earth Planet. Sci. Lett. 298 (1–2), 143–152.
Mienis, F., de Stigter, H.-C., White, M., Duineveld, G., de Haas, H., van Weering, T.C.E., 2007. Hydrodynamic controls on cold-water coral growth and carbonate-mound development at the SW and SE Rockall Trough margin, NE Atlantic Ocean. Deep Sea Res. Part I 54, 1655–1674.
Mienis, F., de Stigter, H.C., de Haas, H., van Weering, T.C.E., 2009. Near-bed particle deposition and resuspension in a cold-water coral mound area at the Southwest Rockall Trough margin, NE Atlantic. Deep Sea Res. Part I 56, 1026–1038.
Millot, C., 1999. Circulation in the Western Mediterranean Sea. J. Mar. Syst. 20, 423–442.
Mohn, C., Rengstorf, A., White, M., Duineveld, G., Mienis, F., Soetaert, K., Grehan, A., 2014. Linking benthic hydrodynamics and Coldwater coral occurrences: a high-resolution model study at three Coldwater coral provinces in the NE Atlantic. Prog. Oceanogr. 122, 92–104.
Navas, J.M., Miller, P.L., Henry, L.-A., Hennige, S.J., Roberts, J.M., 2014. Ecohydrodynamics of Cold-Water Coral Reefs: a Case Study of the Mingulay Reef complex (Western Scotland). PLoS One 9, e98218.
Pardo, E., Rubio, R.A., García, S., Ubero, J., 2011. Documentación de arrecifes de corales de agua fría en el Mediterráneo occidental (Mar de Alborán). Chronica Nat. 20–34.
Pérez-Folgado, M., Sierro, F.J., Flores, J.A., Grimalt, J.O., Zahn, R., 2004. Paleoclimatic variations in foraminifer assemblages from the Alboran Sea (Western Mediterranean) during the last 150 ka in ODP Site 977. Mar. Geol. 212, 113–131.
Pomar, L., Morsilli, M., Hallock, P., Bádenas, B., 2012. Internal waves, an under-explored source of turbulence events in the sedimentary record. Earth Sci. Rev. 111, 56–81.
Puig, P., Palanques, A., Guillén, J., El Khatab, M., 2004. Role of internal waves in the generation of nepheloid layers on the northwestern Alboran slope: implications for continental margin shaping. J. Geophys. Res. Oceans 109, C9.
Raddatz, J., Rüggeberg, A., Liebetrau, V., Foubert, A., Hathorne, E., Fietzke, J., Eisenhauer, A., Dullo, W.-C., 2014. Environmental boundary conditions of cold-water coral mound growth over the last 3 million years in the Porcupine Seabight, Northeast Atlantic. Deep Sea Res. Part II 99, 227–236.
Ramos, A., Sanz, J.L., Ramil, F., Agudo, L.M., Presas-Navarro, C., 2017. The Giant Cold-Water Coral Mounds Barrier off Mauritania. In: Ramos, A., Ramil, F., Sanz, J.L. (Eds.), Deep-Sea Ecosystems off Mauritania: Research of Marine Biodiversity and Habitats in the Northwest African Margin. Springer Netherlands, Dordrecht, p. 659.
Rasmussen, S.O., Bigler, M., Blockley, S.P., Blunier, T., Buchardt, S.L., Clausen, H.B., Cvijanovic, I., Dahl-Jensen, D., Johnsen, S.J., Fischer, H., Gkinis, V., Guillevic, M., Hoek, W.Z., Lowe, J.J., Pedro, J.B., Popp, T., Seierstad, I.K., Steffensen, J.P., Svensson, A.M., Vallelonga, P., Vinther, B.M., Walker, M.J.C., Wheatley, J.J., Winstrup, N., 2014. A stratigraphic framework for abrupt climatic changes during the last Glacial period based on three synchronized Greenland ice-core records: refining and extending the INTIMATE event stratigraphy. Quat. Sci. Rev. 106, 14–28.
Reimer, P.J., Bard, E., Bayliss, A., Beck, J.W., Blackwell, P.G., Ramsey, C.B., Buck, C.E., Cheng, H., Lawrence Edwards, R., Friedrich, M., Grootes, P.M., Guilderson, T.P., Haflidason, H., Hajdas, I., Hatté, C., Heaton, T.J., Hoffmann, D.L., Hogg, A.G., Hughen, K.A., Kaiser, K.F., Kromer, B., Manning, S.W., Niu, M., Reimer, R.W., Richards, D.A., Scott, E.M., Southon, J.R., Staff, R.A, Turney, C.S.M., van der Plicht, J., 2013. IntCal13 and Marine13 Radiocarbon Age Calibration Curves 0–50,000 years cal BP. Radiocarbon 55, 1869–1887.
Remia, A., Taviani, M., 2005. Shallow-buried Pleistocene Madrepora-dominated coral mounds on a muddy continental slope. Tuscan Archipelago, NE Tyrrhenian Sea, Facies 50, 419–425.
Roberts, J.M., Wheeler, A.J., Freiwald, A., 2006. Reefs of the deep: the Biology and Geology of Cold-Water Coral Ecosystems. Science 312, 543–547.
Roberts, J.M., Wheeler, A.J., Freiwald, A., Cairns, S., 2009. Cold-Water Corals. Cambridge University Press, p. 334.
Robinson, L.F., Henderson, G.M., Hall, L., Matthews, I., 2004. Climatic control of riverine and seawater uranium-isotope ratios. Science 305, 851–854.
Rodrigo-Gámiz, M., Martínez-Ruiz, F., Jiménez-Espejo, F.J., Gallego-Torres, D., Nieto-Moreno, V., Romero, O., Ariztegui, D., 2011. Impact of climate variability in the western Mediterranean during the last 20,000 years: oceanic and atmospheric responses. Quat. Sci. Rev. 30, 2018–2034.
Rogerson, M., Cacho, I., Jimenez-Espejo, F., Reguera, M.I., Sierro, F.J., Martinez-Ruiz, F., Frigola, J., Canals, M., 2008. A dynamic explanation for the origin of the western mediterranean organic-rich layers. Geochem. Geophys. Geosyst. 9.
Rosso, A., 2005. Bryozoan facies in deep-sea Pleistocene environments of southern Italy. In: Bryozoan Studies: Proceedings of the 13th International Bryozoology Association conference. AA Balkema Publishers, pp. 257–269.
Rosso, A., Di Geronimo, I., 1998. Deep-sea Pleistocene Bryozoa of Southern Italy. Geobios 31, 303–317.
Rosso, A., Di Martino, E., 2016. Bryozoan diversity in the Mediterranean Sea: an update. Mediterr. Mar. Sci. 17 (2), 567–607.
Rüggeberg, A., Dorschel, B., Dullo, W.-C., Hebbeln, D., 2005. Sedimentary patterns in the vicinity of a carbonate mound in the Hovland Mound Province, northern Porcupine Seabight. In: Freiwald, A., Roberts, J.M. (Eds.), Cold-Water Corals and Ecosystems. SpringerVerlag, Berlin Heidelberg, p. 1243.

Rüggeberg, A., Dullo, W.-C., Dorschel, B., Hebbeln, D., 2007. Environmental changes and growth history of a cold-water carbonate mound (Propeller Mound, Porcupine Seabight). Int. J. Earth Sci. 96, 57–72.
Sánchez-Guillamón, O., Rueda, J.L., Wienberg, C., Ercilla, G., Vázquez, J.T., Gómez-Ballesteros, M., Urra, J., Moya-Urbano, E., Estrada, F., Hebbeln, D., 2022. Morphosedimentary, Structural and Benthic Characterization of Carbonate Mound Fields on the Upper Continental Slope of the Northern Alboran Sea (Western Mediterranean). Geosciences 12, 111.
Schröder-Ritzrau, A., Freiwald, A., Mangini, A., 2005. U/Th-dating of deep-water corals from the eastern North Atlantic and the western Mediterranean Sea. In: Freiwald, A., Roberts, J.M. (Eds.), Cold-Water Corals and Ecosystems. SpringerVerlag, Berlin Heidelberg, p. 1243.
Schroeder, K., Garcìa-Lafuente, J., Josey, S.A., Artale, V., Nardelli, B.B., Carrillo, A., Gačić, M., Gasparini, G.P., Herrmann, M., Lionello, P., Ludwig, W., Millot, C., Özsoy, E., Pisacane, G., Sánchez-Garrido, J.C., Sannino, G., Santoleri, R., Somot, S., Struglia, M., Stanev, E., Taupier-Letage, I., Tsimplis, M.N., Vargas-Yáñez, M., Zervakis, V., Zodiatis, G., 2012. Circulation of the mediterranean sea and its variability. In: Lionello, P. (Ed.), The Climate of the Mediterranean Region. Elsevier, Oxford, p. 593.
Siani, G., Paterne, M., Arnold, M., Bard, E., Métivier, B., Tisnerat, N., Bassinot, F., 2000. Radiocarbon reservoir ages in the mediterranean sea and black sea. Radiocarbon 42, 271–280.
Siani, G., Paterne, M., Michel, E., Sulpizio, R., Sbrana, A., Arnold, M., Haddad, G., 2001. Mediterranean Sea surface radiocarbon reservoir age changes since the last Glacial Maximum. Science 294.
Sneli, J.-A., 2014. Nasjonal Marin Verneplan, Skarnsundet i Nord-Trøndelag - Rapport om Marin Fauna. NTNU, Institute of Biology, Trondheim.
Stalder, C., Vertino, A., Rosso, A., Rüggeberg, A., Pirkenseer, C., Spangenberg, J.E., Spezzaferri, S., Camozzi, O., Rappo, S., Hajdas, I., 2015. Microfossils, a key to unravel cold-water carbonate mound evolution through time: evidence from the eastern alboran sea. PLoS One 10, e0140223.
Stalder, C., El Kateb, A., Vertino, A., Rüggeberg, A., Camozzi, O., Pirkenseer, C.M., Spangenberg, J.E., Hajdas, I., Van Rooij, D., Spezzaferri, S., 2018. Large-scale paleoceanographic variations in the western Mediterranean Sea during the last 34,000 years: from enhanced cold-water coral growth to declining mounds. Mar. Micropaleontol. 143, 46–62.
Stuiver, M., Reimer, P., 1993. Extended ^{14}C data base and revised CALIB 3.0 ^{14}C age calibration program. Radiocarbon 35, 215–230.
Stuiver, M., Reimer, P.J., Reimer, R.W., 2019. CALIB 7.1′. Accessed 2019-5-13. http://calib.org.
Tanhua, T., Hainbucher, D., Schroeder, K., Cardin, V., Álvarez, M., Civitarese, G., 2013. The Mediterranean Sea system: a review and an introduction to the special issue. Ocean Sci. 9, 789–803.
Taylor, P.D., Allison, P.A., 1998. Bryozoan carbonates through time and space. Geology 26, 459–462.
Thiem, Ø., Ravagnan, E., Fosså, J.H., Berntsen, J., 2006. Food supply mechanisms for cold-water corals along a continental shelf edge. J. Mar. Syst. 60, 207–219.
Thierens, M., Titschack, J., Dorschel, B., Huvenne, V.A.I., Wheeler, A.J., Stuut, J.B., O'Donnell, R., 2010. The 2.6 Ma depositional sequence from the Challenger cold-water coral carbonate mound (IODP Exp. 307): sediment contributors and hydrodynamic palaeo-environments. Mar. Geol. 271, 260–277.
Titschack, J., Thierens, M., Dorschel, B., Schulbert, C., Freiwald, A., Kano, A., Takashima, C., Kawagoe, N., Li, X., 2009. Carbonate budget of a cold-water coral mound (Challenger Mound, IODP Exp. 307). Mar. Geol. 259, 36–46.
Titschack, J., Fink, H.G., Baum, D., Wienberg, C., Hebbeln, D., Freiwald, A., 2016. Mediterranean cold-water corals – an important regional carbonate factory? Deposit. Rec. 2, 74–96.
Van der Land, C., Eisele, M., Mienis, F., Haas, H., Hebbeln, D., Reijmer, J., Van Weering, T., 2013. Carbonate mound development in contrasting settings on the Irish margin. Deep Sea Res. Part II 99, 297–306.
Van Rooij, D., Hebbeln, D., Comas, M., Vandorpe, T., Delivet, S., the MD194 Shipboard Scientists, 2013. EuroFLEETS Cruise Summary Report "MD194 GATEWAY", Cádiz (ES) - Lissabon (PT), 10–21 June 2013. Ghent University, Belgium, p. 214.
Wagner, H., Purser, A., Thomsen, L., Jesus, C.C., Lundälv, T., 2011. Particulate organic matter fluxes and hydrodynamics at the Tisler cold-water coral reef. J. Mar. Syst. 85, 19–29.
Wang, H., Lo Iacono, C., Wienberg, C., Titschack, J., Hebbeln, D., 2019. Cold-water coral mounds in the southern Alboran Sea (western Mediterranean Sea): internal waves as an important driver for mound formation since the last deglaciation. Mar. Geol. 412, 1–18.
Wang, H., Titschack, J., Wienberg, C., Korpanty, C., Hebbeln, D., 2021. The importance of ecological accommodation space and sediment supply for cold-water coral mound formation, a case study from the western Mediterranean Sea. Front. Mar. Sci. 8, 760909.
Weedon, M.J., Taylor, P.D., 2008. Skeletal ultrastructure and phylogeny of cyclostome bryozoans. Zool. J. Linnean Soc. 128, 337–399.
Wefing, A.-M., Arps, J., Blaser, P., Wienberg, C., Hebbeln, D., Frank, N., 2017. High precision U-series dating of scleractinian cold-water corals using an automated chromatographic U and Th extraction. Chem. Geol. 475, 140–148.
Wheeler, A.J., Beyer, A., Freiwald, A., de Haas, H., Huvenne, V.A.I., Kozachenko, M., Olu-Le Roy, K., Opderbecke, J., 2007. Morphology and environment of cold-water coral carbonate mounds on the NW European margin. Int. J. Earth Sci. 96, 37–56.
White, M., 2007. Benthic dynamics at the carbonate mound regions of the Porcupine Sea Bight continental margin. Int. J. Earth Sci. 96 (1), 1–9.
White, M., Mohn, C., de Stigter, H., Mottram, G., 2005. Deep-water coral development as a function of hydrodynamics and surface productivity around the submarine banks of the Rockall Trough, NE Atlantic. In: Freiwald, A., Roberts, J.M. (Eds.), Cold-Water Corals and Ecosystems. SpringerVerlag, Berlin Heidelberg, p. 1243.
Wienberg, C., 2019. A deglacial cold-water coral boom in the Alboran sea: from coral mounds and species dominance. In: Orejas, C., Jimenez, C. (Eds.), Mediterranean Cold-Water Corals: Past, Present and Future. Springer, pp. 57–60.
Wienberg, C., Hebbeln, D., Fink, H.G., Mienis, F., Dorschel, B., Vertino, A., López Correa, M., Freiwald, A., 2009. Scleractinian cold-water corals in the Gulf of Cádiz - first clues about their spatial and temporal distribution. Deep Sea Res. Part I 56, 1873–1893.
Wienberg, C., Frank, N., Mertens, K.N., Stuut, J.-B., Marchant, M., Fietzke, J., Mienis, F., Hebbeln, D., 2010. Glacial cold-water coral growth in the Gulf of Cádiz: implications of increased palaeo-productivity. Earth Planet. Sci. Lett. 298, 405–416.
Wienberg, C., Titschack, J., Freiwald, A., Frank, N., Lundälv, T., Taviani, M., Beuck, L., Schröder-Ritzrau, A., Krengel, T., Hebbeln, D., 2018. The giant Mauritanian cold-water coral mound province: oxygen control on coral mound formation. Quat. Sci. Rev. 185, 135–152.
Wienberg, C., Titschack, J., Frank, N., De Pol-Holz, R., Fietzke, J., Eisele, M.H., Kremer, A., Hebbeln, D., 2020. Deglacial upslope shift of NE Atlantic intermediate waters controlled slope erosion and cold-water coral mound formation (Porcupine Seabight, Irish margin). Quat. Sci. Rev. 237, 106310.
Wienberg, C., Krengel, T., Frank, N., Wang, H., Van Rooij, D., Hebbeln, D., 2022. Cold-water coral mounds in the western Mediterranean Sea: New insights into their initiation and development since the Mid-Pleistocene in response to changes of African hydroclimate. Quat. Sci. Rev. 293, 107723.
Wood, A.C.L., Probert, P.K., Rowden, A.A., Smith, A.M., 2012. Complex habitat generated by marine bryozoans: a review of its distribution, structure, diversity, threats and conservation. Aquat. Conserv. Mar. Freshwat. Ecosyst. 22, 547–563.
Zabala, M., Maluquer, P., Harmelin, J.-G., 1993. Epibiotic bryozoans on deep-water scleractinian corals from the Catalonia slope (western Mediterranean, Spain, France). Sci. Mar. 57, 65–78.
Zibrowius, H., 1980. Les Scléractiniaires de la Méditerranée et de l'Atlantique nord-oriental. Mémoires de l'Institut océanographique, Monaco.
Zibrowius, H., 1984. Taxonomy in ahermatypic scleractinian corals. Paleontograph. Americana 54, 80–85.